Defense Nuclear Agency
Alexandria, VA 22310-3398

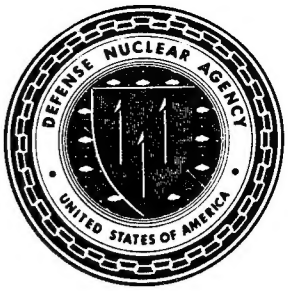

DNA-TR-94-39

Experimental Determination of Probability Distributions for Parameters of a Salem Limestone Cap Plasticity Model

Arlo F. Fossum
Tom W. Pfeifle
Kirby D. Mellegard
RE/SPEC Incorporated
P.O. Box 725
Rapid City, SD 57709

January 1995

Technical Report

CONTRACT No. DNA 001-92-C-0030

DISCLAIMER

REVIEW OF THIS MATERIAL DOES NOT IMPLY DEPARTMENT OF DEFENSE ENDORSEMENT OF FACTUAL ACCURACY OR OPINION.

Destroy this report when it is no longer needed. Do not return to sender.

PLEASE NOTIFY THE DEFENSE NUCLEAR AGENCY, ATTN: CSTI, 6801 TELEGRAPH ROAD, ALEXANDRIA, VA 22310-3398, IF YOUR ADDRESS IS INCORRECT, IF YOU WISH IT DELETED FROM THE DISTRIBUTION LIST, OR IF THE ADDRESSEE IS NO LONGER EMPLOYED BY YOUR ORGANIZATION.

DISTRIBUTION LIST UPDATE

This mailer is provided to enable DNA to maintain current distribution lists for reports. (We would appreciate your providing the requested information.)

NOTE:
Please return the mailing label from the document so that any additions, changes, corrections or deletions can be made easily. For distribution cancellation or more information call DNA/IMAS (703) 325-1036.

☐ Add the individual listed to your distribution list.

☐ Delete the cited organization/individual.

☐ Change of address.

NAME: _____

ORGANIZATION: _____

OLD ADDRESS	CURRENT ADDRESS
_____	_____
_____	_____
_____	_____

TELEPHONE NUMBER: ( ) _____

DNA PUBLICATION NUMBER/TITLE	CHANGES/DELETIONS/ADDITIONS, etc.) *(Attach Sheet if more Space is Required)*
_____	_____
_____	_____
_____	_____

DNA OR OTHER GOVERNMENT CONTRACT NUMBER: _____

CERTIFICATION OF NEED-TO-KNOW BY GOVERNMENT SPONSOR (if other than DNA):

SPONSORING ORGANIZATION: _____

CONTRACTING OFFICER OR REPRESENTATIVE: _____

SIGNATURE: _____

CUT HERE AND RETURN

DEFENSE NUCLEAR AGENCY
ATTN: IMAS
6801 TELEGRAPH ROAD
ALEXANDRIA, VA 22310-3398

DEFENSE NUCLEAR AGENCY
ATTN: IMAS
6801 TELEGRAPH ROAD
ALEXANDRIA, VA 22310-3398

REPORT DOCUMENTATION PAGE	Form Approved OMB No. 0704-0188

1. AGENCY USE ONLY (Leave blank)	2. REPORT DATE	3. REPORT TYPE AND DATES COVERED
	950101	Technical 920131 - 940630

4. TITLE AND SUBTITLE

Experimental Determination of Probability Distributions for Parameters of a Salem Limestone Cap Plasticity Model

5. FUNDING NUMBERS

C -DNA 001-92-C-0030
PE -62715H
PR -AC
TA -AB
WU-DH316140

6. AUTHOR(S)

Arlo F. Fossum, Tom W. Pfeifle and Kirby D. Mellegard

7. PERFORMING ORGANIZATION NAME(S) AND ADDRESS(ES)

RE/SPEC Incorporated
P.O. Box 725
Rapid City, SD 57709

8. PERFORMING ORGANIZATION REPORT NUMBER

RSI-0502

9. SPONSORING/MONITORING AGENCY NAME(S) AND ADDRESS(ES)

Defense Nuclear Agency
6801 Telegraph Road
Alexandria, VA 22310-3398
SPSD/Senseny

10. SPONSORING/MONITORING AGENCY REPORT NUMBER

DNA-TR-94-39

11. SUPPLEMENTARY NOTES

This work was sponsored by the Defense Nuclear Agency under RDT&E RMC Code B4662D AC AB 00001 4300A 25904D.

12a. DISTRIBUTION/AVAILABILITY STATEMENT

Approved for public release; distribution is unlimited.

12b. DISTRIBUTION CODE

13. ABSTRACT (Maximum 200 words)

Marginal probability density functions and a correlation matrix are determined for parameters of the Weidlinger cap plasticity model for Salem limestone specimens originating from Bedford, Indiana. The report describes a program comprising precision laboratory testing, parameter estimation, and probability distribution model fitting. A novel testing scheme allows a complete set of material parameters to be determined from a single test specimen. Statistical properties and distributions are determined by replication. The fitted model is validated by predicting loading histories not included in the fitting database.

The testing program includes uniaxial strain tests in axial strain control (-1×10^{-6}/s), unconfined compression tests in axial strain control (-1×10^{-5}/s), hydrostatic compression tests in load control (-0.02 MPa/s), and triaxial compression tests in axial strain control (-1×10^{-5}/s) during loading and load control during unloading (-0.02 MPa/s). All specimens are tested at a constant temperature of 20°C and at a water saturation level of 50%.

14. SUBJECT TERMS		15. NUMBER OF PAGES
Salem Limestone	Parameter Estimation	60
Laboratory Testing	Probability Density Functions	16. PRICE CODE

17. SECURITY CLASSIFICATION OF REPORT	18. SECURITY CLASSIFICATION OF THIS PAGE	19. SECURITY CLASSIFICATION OF ABSTRACT	20. LIMITATION OF ABSTRACT
UNCLASSIFIED	UNCLASSIFIED	UNCLASSIFIED	SAR

CLASSIFIED BY:	N/A since Unclassified.
DECLASSIFY ON:	N/A since Unclassified.

13. ABSTRACT (Continued)

The validation study clearly demonstrates that the parameter estimation procedure produces high-quality parameter values, and that the fitted model can not only reproduce measured data included in the fitting database, but also predicts responses from tests conducted under loading histories different from those found in the fitting database.

SUMMARY

The DNA Underground Technology Program (UTP) is developing a method to predict structural hardness for use in survivability and vulnerability assessments of underground facilities. This method is proceeding through a combination of theoretical, analytical, and experimental activities. As part of the UTP experimental program, DNA contracted RE/SPEC Inc. to perform laboratory-scale tests on intact sedimentary rock. This work is motivated by the need to analyze underground structures probabilistically to account for the large amount of scatter in mechanical properties exhibited by rock and the uncertainty in site characterization and imprecision in loads. The overall objectives of this laboratory testing program are to

1. Develop a constitutive model for intact sedimentary rock (i.e., Salem Limestone) that is valid for the large strain, large shear stress, low pressure (<150 MPa confining pressure), and complex strain histories expected in the rock immediately surrounding deep tunnels subjected to ground-shock loading; and to,
2. Construct a database adequate for DNA to develop a probabilistic constitutive model for intact sedimentary rock.

Marginal probability density functions and a correlation matrix were determined for the parameters of the Weidlinger cap plasticity model. This information is sufficient to transform non-normal correlated random variables into statistically independent normal ones. The experimental program comprised precision laboratory testing, parameter estimation, and probability distribution model fitting. A novel testing scheme allowed a complete set of material parameters to be determined from a single test specimen. Statistical properties and distributions were determined by replication. The fitted model was validated by predicting loading histories not included in the fitting database. The validation results clearly demonstrated that the parameter estimation procedure produced high-quality parameter values, and that the fitted model could not only reproduce measured data included in the fitting database, but also that it could predict responses from tests conducted under loading histories different from those found in the fitting database.

PREFACE

This work was conducted under Contract DNA 001-92-C-0030. The technical monitor was Dr. Paul E. Senseny.

The authors are grateful for the technical input offered by Ben Thacker of Southwest Research Institute, Jim Gran of SRI International, Jack Trulio of Applied Theory, Inc. and Tom Pučik of Logicon RDA.

CONVERSION TABLE

Conversion factors for U.S. Customary to metric (SI) units of measurement.

MULTIPLY ⟶ BY ⟶ TO GET

TO GET ⟵ BY ⟵ DIVIDE

foot	3.048 000 x E-1	meter (m)
inch	2.540 000 x E-2	meter (m)
pound-force (lbs avoirdupois)	4.448 222	newton (N)
pound-force/inch^2 (psi)	6.894 757	kilo pascal (kPa)
pound-mass (lbm avoirdupois)	4.535 924 x E-1	kilogram (kg)

TABLE OF CONTENTS

FIGURES

TABLES

SECTION 1

INTRODUCTION

High-quality solutions to complex underground structural mechanics problems require that constitutive relations be sufficiently realistic and that uncertainties be understood and quantified. There are several types of uncertainties. Uncertainty can be categorized as (1) inherent (variability inherent in the material or environment), (2) statistical (incompleteness of statistical data), (3) modeling (use of simplified models), and (4) human (errors, quality, judgment). Only inherent uncertainty is irreducible. A probabilistic approach can be used to treat both irreducible and reducible uncertainties. Irreducible uncertainties can be modeled as random variables. Reducible uncertainties can be treated by assuming that the mean and standard deviation of the reducible random variables are random, which results in a confidence bound to the calculated probability. In this report we deal only with inherent material variability to account for the large amount of scatter in the mechanical properties exhibited by rock. Constitutive models for porous sedimentary materials are reasonably well developed and can simulate a variety of phenomena such as extension fracture in tension, shear failure under deviatoric stresses, and pore collapse under compressive mean stresses. Cap plasticity models represent this type of behavior. Constitutive equations under the category of cap plasticity models have been formulated by numerous authors, e.g., Drucker et al. (1957), DiMaggio and Sandler (1971), Miller and Cheatham (1972), Baron et al. (1973), Baladi and Hadala (1974), Sandler et al. (1976), Sandler (1976), Sandler and Rubin (1979), Yamada and Abou-Sayed (1979), Baladi and Rohani (1979), Celle and Cheatham (1981), Cheatham et al. (1984), Katona (1984), Katona and Mulert (1984), Resende and Martin (1985), McCarron and Chen (1987), Chu and Brandt (1987), Simo et al. (1988), Huang and Chen (1990), Rubin (1990), Abduljauwad et al. (1992), Hofstetter et al. (1993), and Schwer and Murray (1994). Cap models developed by these authors describe material behavior ranging from very simple to very complex. Some of the more complex features include material behavior at finite strain, anisotropy, rate dependence, nonlinear isotropic and kinematic hardening of shear and volumetric initial yield surfaces (compacting and dilating), pore pressure, and Lode-angle dependence of yield surfaces.

Procedures for cap model fitting are described by several of the authors cited. Laboratory tests used most often include uniaxial strain, triaxial compression, and hydrostatic

compression tests. Some of the more sophisticated material models require cyclic stress-strain and high strain-rate tests.

In the traditional approach, material parameters are evaluated sequentially. For example, the unloading portion of a hydrostatic compression test (slope of pressure versus volumetric-strain curve) is used to determine the bulk modulus; the unloading portion of a triaxial compression test (slope of stress-difference versus strain-difference curve) is used to determine the shear modulus; a series of proportional loading or constant mean stress triaxial compression tests is used to establish a shear yield envelope. Parameter estimation procedures fit a shear yield (or failure) function to these data. With elastic and shear yield parameters held fixed, the remaining parameters of the cap portion of the model are determined by an iterative (trial-and-error) simulation procedure; i.e., a cap shape and hardening rule are postulated and the behavior of the model calculated and compared to measured material data from uniaxial strain, triaxial compression, or hydrostatic compression tests. This type of fitting approach gives approximate physical interpretation to some or all of the parameters.

Nevertheless, at least three deficiencies plague the traditional approach. First, the data matrix requires a relatively high number of laboratory tests and therefore a high number of test specimens. For example, a three-parameter shear yield function requires at least three triaxial compression or proportional loading tests to determine the parameters uniquely. However, many more than three tests are usually needed because of data scatter. The American Society for Testing and Materials (ASTM Standard D 2664, 1989) recommends that at least nine tests be conducted at different confining pressures to determine a single set of shear-strength properties. Similar arguments hold for tests required to evaluate the remaining parameters. A second weakness is that errors in values of the first parameters evaluated propagate into values of subsequent parameters. Parameter values may therefore depend on the order in which they are determined. The third disadvantage is that the traditional approach does not permit evaluation of the statistical correlation that may exist among parameters.

These issues pose significant problems when seeking material-parameter probability density functions. If the traditional approach were used as the estimation procedure to compute point estimates of parameters and replication used to determine statistical

properties, the whole series of experiments would have to be repeated many times and the estimation procedure applied to each data set in turn to form a large sample drawn from the sampling distribution. Such a procedure would clearly include a prohibitive number of tests, requiring hundreds of specimens.

The report summarizes recent efforts to determine marginal probability distributions and the correlation among material parameters of a Salem limestone cap plasticity model. The cap model is the one proposed originally by DiMaggio and Sandler (1971), generalized by Sandler et al. (1976), and modified by Sandler and Rubin (1979). The authors devised a testing scheme and parameter estimation procedure allowing all the material parameters to be determined from a single specimen. Comparisons of predictions against measurements from other test types (e.g. uniaxial strain tests) and from tests performed under loading histories different from those found in the fitting database (e.g. triaxial compression tests conducted at different confining pressures) validate the procedure. Probability density functions are determined from twenty replicate tests providing data to construct histograms for each cap model parameter. The Kolmogorov-Smirnov (K-S) test (see Ang and Tang, 1975) measures relative goodness-of-fit among candidate probability distribution functions. Distributions are identified that best characterize the parameter histograms. Also determined is the matrix of correlation coefficients giving the degree of correlation among the parameters.

From a practical standpoint, results of this study will be key in underground probabilistic structural analyses. While it is generally conceded that a full Monte Carlo solution is impractical for large-scale underground calculations, considerable progress has been made in the development and use of approximate analytical methods. Notable among these are reliability analysis methods for geotechnical applications based on Most Probable Point Locus (MPPL) concepts in which Fast Probability Integration (FPI) is used to estimate the most probable combination of random variables that lead to failure (for examples in the use of this technique for geotechnical applications see Harren and Fossum, 1991; Fossum et al., 1991; and Fossum and Munson, 1994). Advanced mean value iteration techniques compute converged MPPL and estimate probability of failure. These methods are accurate relative to Monte Carlo results even in the tails of the distributions. Where a Monte Carlo analysis might require 100,000 deterministic solutions, the FPI method might require as few as 50 deterministic solutions. It is important to note, however, that these FPI methods require

that the random variables be normally distributed and statistically independent. If the random variables, such as the constitutive parameters, are non-normal correlated variables, they must be transformed to statistically independent normal variables. This can be achieved if marginal distributions *and* the correlation matrix for the parameters are known. The results obtained in this report are sufficient for this purpose.

The remainder of the report describes the cap plasticity model, experimental program, and the procedures used to evaluate the parameters, their statistical correlations, and distributions. A discussion of results follows including those of a validation study.

SECTION 2

CAP PLASTICITY MODEL

A detailed description and a solution algorithm for the cap plasticity model can be found in Sandler and Rubin (1979). Because the imposed test conditions were known precisely, it was possible to construct a response model corresponding to each test. All of the tests were conducted in an axially-symmetric compression machine giving rise to triaxial compression stress states. Using a negative sign convention for compression and denoting the maximum, intermediate, and minimum principal stresses as σ_1, σ_2, σ_3 respectively, a state of triaxial compression is said to exist when

$$\sigma_1 = \sigma_2 > \sigma_3 \tag{2.1}$$

A lateral confining pressure in the testing machine corresponds to $\sigma_1 = \sigma_2$, while the imposed axial stress is equal to σ_3. The square root of the second invariant of deviator stress, $\sqrt{J_2}$, in this system, becomes

$$\sqrt{J_2} = \frac{\Delta\sigma}{\sqrt{3}} \tag{2.2}$$

where the stress difference, $\Delta\sigma$, is the difference between the confining pressure and the imposed axial stress, $\Delta\sigma = \sigma_1 - \sigma_3$. The first stress invariant, I_1, is defined by

$$I_1 = \sigma_1 + \sigma_2 + \sigma_3 = 3P \tag{2.3}$$

where P denotes "mean pressure."

The cap model (Sandler and Rubin, 1979) was formulated in terms of two invariants, I_1 and J_2. A three invariant model is generally required for rocks and similar brittle materials such as concrete. If a model with more than two invariants is used, these invariants can also be expressed in terms of the imposed test conditions. However, depending upon the functional form of such a model, additional tests may be needed (but not necessarily) in more than just triaxial compression stress states to evaluate all of the material parameters. In our study, we used Equations 2.2 and 2.3 to develop response models in terms of the imposed test conditions since all data were obtained at the same Lode angle, which corresponds to triaxial compression.

The model can be used to model elastic behavior, shear failure, and cap plasticity. The model is a classical rate-independent, associative plasticity model in which the yield surface consists of a shear yield surface and a hardening cap as illustrated in Figure 2-1. In our work we have chosen to fix the shear yield surface. While this surface has been called a shear failure surface, it is more correctly termed a limit-state or ultimate-shear-yield surface. Holding this surface fixed is not a necessary model restriction. If experimental data warrant, a hardening shear surface can be included as part of the complete model. Linear elastic behavior occurs when the stress is within the composite shear-failure and yield-cap surfaces. The two elastic constants determined from the test data are the bulk modulus, K, and the shear modulus, G.

When the stress point lies on the shear-failure envelope, shear failure occurs according to the criterion

$$\frac{\Delta\sigma}{\sqrt{3}} = A - C\exp(3BP) \tag{2.4}$$

where A, B, and C are material constants. During shear failure, the plastic strain comprises a shear component and a volumetric (dilatant) component.

When the stress point lies on the cap and pushes it outward, plastic strain comprises an irreversible decrease in volume called compaction, and a shear component for other than pure hydrostatic compression stress states. The cap motion is related to the plastic decrease in volume through a hardening rule. The shape of the cap is described as an elliptical surface defined by

$$\frac{\Delta\sigma}{\sqrt{3}} = \frac{1}{R}\sqrt{[X(\kappa) - L(\kappa)]^2 - [3P - L(\kappa)]^2} \tag{2.5}$$

in which

$$L(\kappa) = \begin{cases} \kappa \text{ if } \kappa < 0 \\ 0 \text{ if } \kappa \geq 0 \end{cases}; \quad X(\kappa) = \kappa - R[A - C\exp(BL)] \tag{2.6}$$

The cap position parameters $L(\kappa)$ and $X(\kappa)$ locate the current cap surface. The material parameter, R, defines the ratio of principal ellipse radii of the cap surface. The hardening parameter, κ, is defined through a functional of $X(\kappa)$ and volumetric plastic strain, ε_v^p, caused only by cap action,

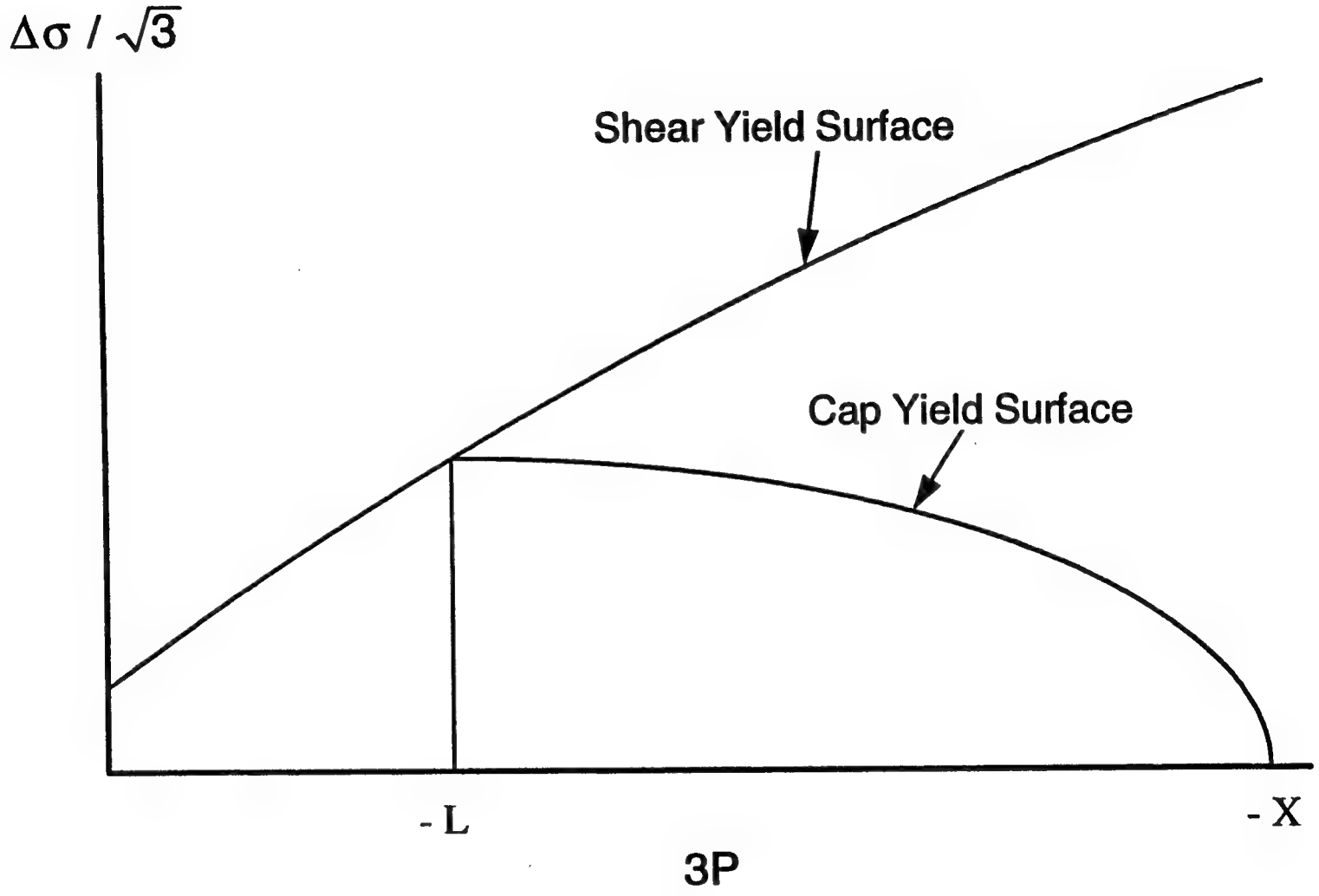

Figure 2-1. Ultimate shear and cap yield surfaces of the cap plasticity model.

$$\overline{\varepsilon_v^p} = W[\exp\{D(X - X_0)\} - 1] \tag{2.7}$$

in which W and D are material parameters, X_0 is the initial cap position, and $\overline{\varepsilon_v^p}$ is a history-dependent functional of ε_v^p given by

$$\overline{\dot{\varepsilon}_v^p} \equiv \min(\dot{\varepsilon}_v^p, 0) \tag{2.8}$$

Sandler and Rubin (1979) introduced Equation 2.8 to prevent the cap from retracting.

An important issue that will not be addressed here because it does not affect parameter estimation is the manner in which plastic strain rate is determined when loading develops on both cap and shear yield surfaces. This occurs in the current model at the point of horizontal tangency to the cap ellipse in $\Delta\sigma$ - P space where the cap intersects the shear yield surface. For a more detailed discussion of this issue the interested reader should consult articles by Resende and Martin (1985) and Simo et al. (1988). Load paths in the current work are chosen so that simultaneous loading does not occur on both yield surfaces.

SECTION 3

EXPERIMENTAL PROGRAM

3.1 SPECIMENS.

Salem limestone, also called Spergen, Indiana, and Bedford limestone, is a porous, bioclastic, brecciated, calcite-cemented, medium-strength limestone (ASTM, 1992). Its carbonate phases consist of 69 percent fossiliferous calcite and 31 percent calcite cement. Porosity varies between about 12 percent and 18 percent depending on quarry location. The block sample used for specimen preparation had a density of 2.698 Mg/m^3 and a porosity of 13.2 percent.

Specimens of this rock are fabricated in the form of solid right-circular cylinders having nominal diameters of 55 mm and lengths of 138 mm for length-to-diameter ratios, L:D, of 2.5. The specimens are first cored from large blocks using a conventional rock coring barrel mounted in a vertical milling machine. Then the ends of the cores are finished to final dimensions by cutting each specimen to approximate length in a slabbing saw and trimming the ends in a lathe. Both the coring and cutting operations use water as a coolant. Following the two-step preparation procedure, each specimen is subjected to an acceptance test. The acceptance test includes specifications for flatness (< 0.02 mm), straightness (< 0.3 mm gapping), and perpendicularity (< 0.001 radians). These specifications are more stringent than those given by the ASTM Standard D4543-85 (ASTM, 1988) and were selected to isolate only material variability by reducing specimen dimension uncertainties and eliminating eccentric loading problems for poorly machined specimens. In addition to these stringent dimensional tolerances, the maximum allowable difference between any measured diameter and the average of six measurements taken for three sets of orthogonal diameters at the mid-height and near the specimen ends is not allowed to exceed 0.1 mm. Likewise, the length is not allowed to vary by more than 1.0 mm from the required L:D multiplied by the average diameter. Specimens failing the acceptance test are discarded or remachined until each specification is met.

Specimens are soaked in ordinary tap water for 30 minutes to raise their water saturation level to 50 percent. Each specimen is then placed between two stainless steel

metal endcaps and the endcap-specimen interfaces covered with lengths of 1.75-mm-thick Viton tubing that extend to within 6 mm of the mid-height of the specimen. Two thin, 0.3-mm-thick jackets are placed over the entire specimen-endcap assembly and sealed to the endcaps with lockwire. The inner and outer jackets are fabricated from Viton and latex, respectively. The advantages of this jacketing technique are summarized in the next section.

3.2 LABORATORY TEST SYSTEMS.

The specimens are tested using a computer-controlled, servohydraulic test system, Model 315.03 manufactured by MTS Systems, Inc. The frame and axial load actuator are rated at an axial load capacity of -4.5 MN in compression. The pressure vessel and pressurizing systems used for triaxial compression testing are rated at confining pressures of -150 MPa. The axial force and confining pressure systems operate independently through the use of two separate servo loops that increase, decrease, or maintain loads according to a command signal from a computer that controls the test.

Because mechanical testing provides data to quantify uncertainties in material parameters and because these parameters are used to quantify uncertainties in structural behavior, it is clear that test-induced uncertainties should be small. The authors endeavor to minimize the uncertainty in the data caused by the test system through use of (1) optimal transducer location, (2) automated test control, and (3) appropriate calibration techniques.

Transducer location is very important to these tests. The test machine is equipped with a load cell inside the pressure vessel and extensometry that is mounted directly to the specimen. Frictional forces are eliminated from the load cell reading by placing the load cell inside the vessel as shown in Figure 3-1a. Additionally, the cell is compensated for confining pressure so that its output is nominally zero at hydrostatic stress states. Even at high hydrostatic pressures, a high gain can be applied to the load cell signal to improve resolution of the load measurement and enhance precise axial load control.

Specimen deformation is measured using direct-contact extensometers. Axial and circumferential direct-contact extensometers are mounted to the specimen over the jackets (Figure 3-1b). The circumferential extensometer is placed between the ends of a roller-link chain wrapped about the mid-height of the specimen and measures changes in chord length

defined by the ends of the chain. The initial chord length is typically about 20 mm. The chain is positioned over the two thin jackets but does not contact the thick Viton tubing that covers the specimen-endcap interfaces. Mellegard et al. (1993) have shown that jacket type and thickness have a profound effect on deformation measurements of the circumferential extensometer. Therefore, extensometer measurements are corrected for jacket deformations based on calibrations performed on 6061-T6 aluminum. The axial extensometer has a 50.8-mm gage length which is set to within 0.0125 mm using pins in the opposing arms of the extensometer. Each set of opposing arms is positioned on either side of the specimen so that the gage length of the extensometer is centered over the midheight of the specimen. Contact between the extensometer and specimen occurs through pins located in the arms of the extensometer and held in place with springs. Measurements by the axial extensometer are unaffected by deformation of the protective jacket. The benefit in using extensometers that mount directly to the specimen as shown in Figure 3-1b is that deformations are measured within the zone of rock that is presumed to have a uniform strain field. Further, any non-specimen deformations of the platens, specimen-platen interfaces, or machine distortion are not part of the deformation measurement. As with the load cell, mounting the extensometer directly on the specimen enhances test control because of the increased extensometer signal sensitivity to specimen deformation.

Use of servo-hydraulic testing techniques, implemented and controlled by a preprogrammed computer, greatly reduces uncertainty in the data. One of the main advantages in using a computer is repeatability of loading conditions between specimens. With a non-computerized system, repeatability of loading is limited by operator skill. With a computerized system, the only limit is resolution of the digital device used to produce loading commands. The system used here employs a 12-bit digital-to-analog converter to produce commands that drive the servo-control loops. This provides control resolution of 1 part in 4,096, which means that for a full-scale confining pressure range of -150 MPa, the pressure-level command has a precision of approximately 0.037 MPa.

Of the three actions taken to reduce uncertainty caused by the test system, the most conspicuous one involves calibration. Calibration in this work follows the ANSI/ASME Performance Test Code on Measurement Uncertainty (PTC 19.1) that states that insofar as possible "the calibration process should include a reasonable simulation of instrument test-like conditions." Thus, during calibration, transducers are connected in their normal orientations on the test system and their outputs are recorded through the analog-to-digital converter at the computer. A typical calibration consists of applying twenty known standard

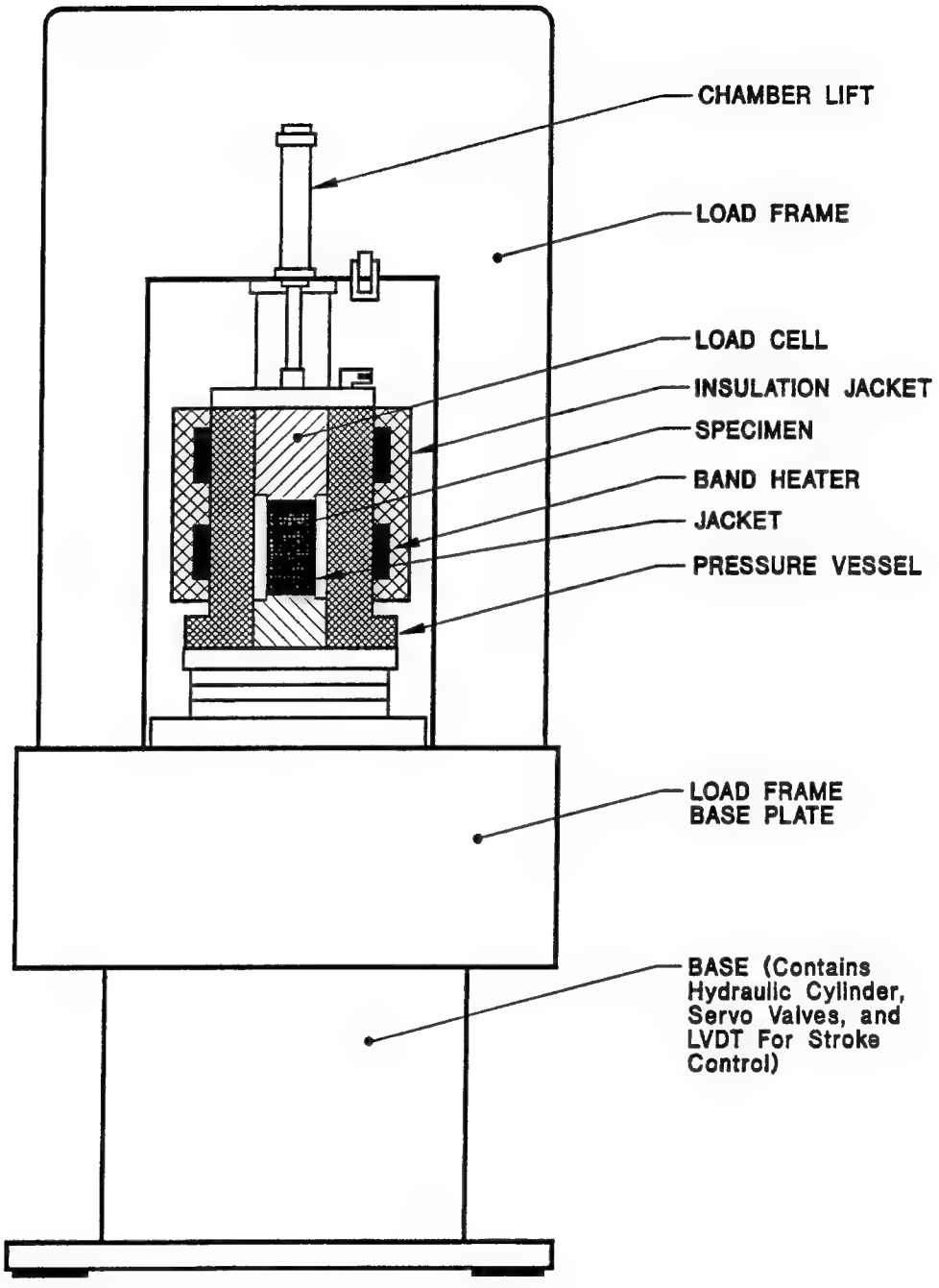

(a) Load frame

Figure 3-1. Schematic of load frame and deformation transducers used for all testing.

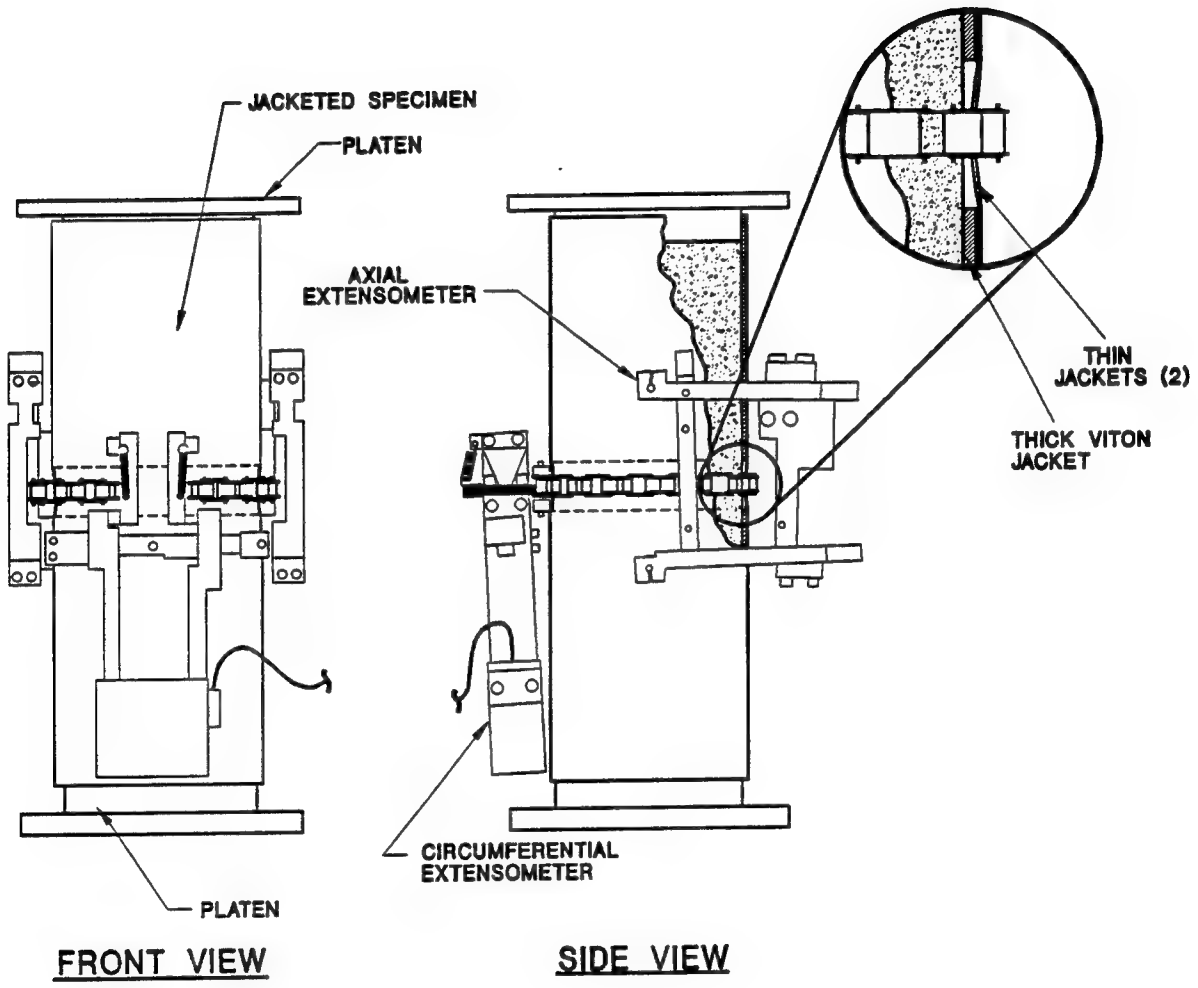

(b) Deformation transducers

Figure 3-1. Schematic of load frame and deformation transducers used for all testing (continued).

inputs to the transducer and reading the corresponding transducer outputs at the data collection point. The correlation between the transducer outputs and known standard inputs provides the sensitivity and offset for that transducer. Standard inputs are provided by standards that are traceable to the U.S. National Institute for Standards and Technology (NIST). The analog-to-digital converter uses 13 bits to digitize the magnitude of the signal and one bit to indicate sign. Thus, measurements are made with a precision of 1 part in 8,192 over full scale and are not limited by resolution. Measurement accuracies, however, are limited by the standards used for calibration and repeatability of the transducers. Calibration verification is performed by determining the difference between indicated readings versus standard input after applying the standard input in 10 equal steps over the calibrated range. The transducer response at each step is predicted using previously determined calibration constants. The process of calibration/verification is acceptable if predicted values fall within 1.0 percent of reading for each step in the verification.

The typical calibration method described above is appropriate for load and confining pressure transducers. The calibrated ranges of these transducers are -2.5 MN and -150 MPa, respectively. The range on load permits measurements of an absolute stress difference to 1,100 MPa for specimens with nominal diameters of 55 mm. The ranges in load and pressure encompass the ranges established by the test matrix. The typical calibration method is also appropriate for deformation transducers, but was modified as described below to improve resolution and accuracy.

The stress ranges required by the test matrix cause large strains that pose a unique experimental problem when used in model fitting efforts aimed at estimating both elastic and plastic model parameters. That problem is how to maintain high resolution and accuracy for measurements of small elastic deformations while simultaneously allowing for the measurements of large plastic deformations. The problem is addressed by first increasing the gain of the signal conditioner that services each deformation extensometer so that a full-scale voltage of 10 volts represents approximately one-tenth of the physical range of each extensometer. This action produces an extensometer output signal that is highly sensitive to small extensometer measurements and very accurate over a small range of specimen deformation. Then, to utilize the full physical ranges of the extensometers for accommodating large plastic strains, a unique feature of the test system is employed that applies an adjustable offset voltage to each signal received from the deformation extensometers. This

adjustable offset voltage is controlled by the system computer and is set to shift the output of the signal conditioner back to zero whenever the level approaches 10 volts. The computer keeps track of the current offset voltage used to shift the signal and applies appropriate calibration factors when converting the data acquisition signal into engineering units. Multiple shifts of the signal will occur to accommodate specimen deformations that approach the full physical ranges of the extensometers.

The technique of amplifying the extensometer signal and then offsetting the signal conditioner output provides superb sensitivity in test control and greater resolution is realized in data acquisition at all levels of deformation and loading. This approach, however, requires a more complex calibration of the extensometers than the typical calibration described previously. A typical transducer calibration involves the determination of only two calibration constants; i.e., the sensitivity and offset. The sensitivity and offset represent the slope and intercept of the line fitted to calibration data pairs comprising standard inputs versus indicated readings. The calibration procedure for the extensometers, however, requires the determination of four calibration constants; two that represent the nominal slope and intercept as determined in a typical calibration, and two more that represent how the nominal slope changes whenever the signal is shifted. The calibration procedure begins by setting the extensometer to its natural null position that represents the beginning of its operating range. At this point, the signal conditioner output will be at zero without any need for external shifting of the signal level. With the signal conditioner gain set for high amplification, a typical calibration run is made over the small range of deformation allowed by the high amplification. At the end of the first typical calibration, the extensometer is positioned at one-tenth of its physical range and the signal conditioner output is 10 volts. This output voltage is then shifted back to zero by applying the external voltage and another typical calibration run is now made with the "null" extensometer position shifted. These steps of calibration and voltage shifting continue until the physical range of the extensometer is reached. This procedure of calibrating over small strain ranges that are concatenated by external voltage shifts to form a large strain range provides enough data to determine all four calibration constants. The full ranges of the axial and circumferential extensometers can handle large plastic strains to -10 percent and 6 percent, respectively.

Although direct-contact transducer measurements are preferable to other types of measurements, their use in the harsh environment of the pressure vessel of the test system

raises questions about the effect of pressure and temperature on the output of transducers. Senseny (1987) has shown that pressure affects only the offset of the extensometers while temperature affects both offset and sensitivity. The effects of pressure on the deformation transducers used in this study were examined and reported by Mellegard et al. (1993). Using their results, the changes in the offsets of the axial and circumferential extensometers are -0.15×10^{-6} m/MPa and 0.42×10^{-6} m/MPa, respectively. The change in the offset of the internal load cell because of pressure is -9.3×10^{-5} MN/MPa. Although all testing is performed at a constant temperature of 20°C in this study, temperature changes of the confining pressure fluid and therefore the direct-contact transducers can occur as a result of adiabatic heating of the confining fluid during pressurization. Mellegard et al. (1993) also studied this phenomenon to examine the effect of pressurization rates on the outputs of direct-contact transducers and concluded that the effects are small provided absolute pressurization rates are less than or equal to 0.02 MPa/s. Therefore, in this study, hydrostatic loading stages are performed at a pressurization rate of -0.02 MPa/s.

3.3 EXPERIMENTAL PROGRAM.

The load history imposed allows the material parameters to be determined from a single test specimen with little uncertainty and generally with minimal confounding among other parameters. The load path includes several stages. Because test conditions in each loading stage are known precisely, response models can be constructed corresponding to each stage. Nonlinear regression can then be used to evaluate the parameters such that the fitted model gives the best fit to the data in a least squares sense. Response models refer to predicted strain in stress-rate control and to predicted stress in total strain-rate control. Simulations of tests follow exactly the load path imposed experimentally.

The first stage of the test is hydrostatic compression in stress-rate control. In this stage, hydrostatic pressure is applied to a cylindrical test specimen at a constant rate of -0.02 MPa/s until -150 MPa is reached. This value is at or near the value needed to initiate plastic volume compaction (pore collapse). Axial and radial strains are measured during the test.

The second stage, triaxial compression loading, begins with a mode switch from stress-rate control to strain-rate control. Radial and tangential stresses, identical from symmetry,

are held constant at -150 MPa while the axial strain is controlled at a constant rate of -1.0 x 10^{-5}/s until an axial strain of -8.5 percent is reached. During this stage radial strain and axial stress are measured. This stage is terminated before the shear surface is reached but only after a major portion of the cap surface has been traversed.

The third stage is unloading with a mode switch back to stress-rate control. Radial and tangential stresses remain constant at -150 MPa while axial stress is reduced to -150 MPa at a constant rate. Axial and radial strains are measured during this stage. Figure 3-2 in $\Delta\sigma$-P space shows the load paths corresponding to these three stages. Figure 3-2 also shows the position of the yield surfaces relative to the load paths. After these first three stages, the measured stress-strain data provide sufficient information to evaluate sensitivity of simulated responses to changes in elastic and cap parameters.

To obtain data sufficient to define the shear yield function parameters, the next portion of the test includes a series of hydrostatic-unload/triaxial-load stages that we term a "walkdown." The test specimen is unloaded hydrostatically from the hydrostatic stress state that existed after the third stage (-150 MPa). When a hydrostatic stress state of -40 MPa is reached, the specimen is loaded in axial strain-rate control until the axial stress stops increasing. The specimen is then unloaded to a hydrostatic stress level of -40 MPa. The specimen is then unloaded hydrostatically to -35 MPa and the process repeated. Five data points are collected during this "walkdown" procedure in -5 MPa hydrostatic increments.

Stress-strain data from the first three stages and the "walkdown" strength data provide sufficient information, from a single specimen, to determine all nine parameters of the cap plasticity model. Statistical properties and sampling distributions for the material parameters follow from replicate testing with 20 specimens.

The 20 replicate tests are part of a larger testing program conducted to characterize the rate-independent deformation of Salem limestone. The larger program comprises 87 hydrostatic/triaxial compression tests and 10 uniaxial strain tests. In addition to the 20 tests performed at a confining pressure of -150 MPa, the hydrostatic/triaxial compression test matrix includes 20 unconfined tests, 10 tests each at -50 MPa and -100 MPa, and one test at each 5 MPa confining pressure increment between -5 MPa and -145 MPa. These tests and the uniaxial strain tests provide data for model validation and are not used in the parameter estimation procedure.

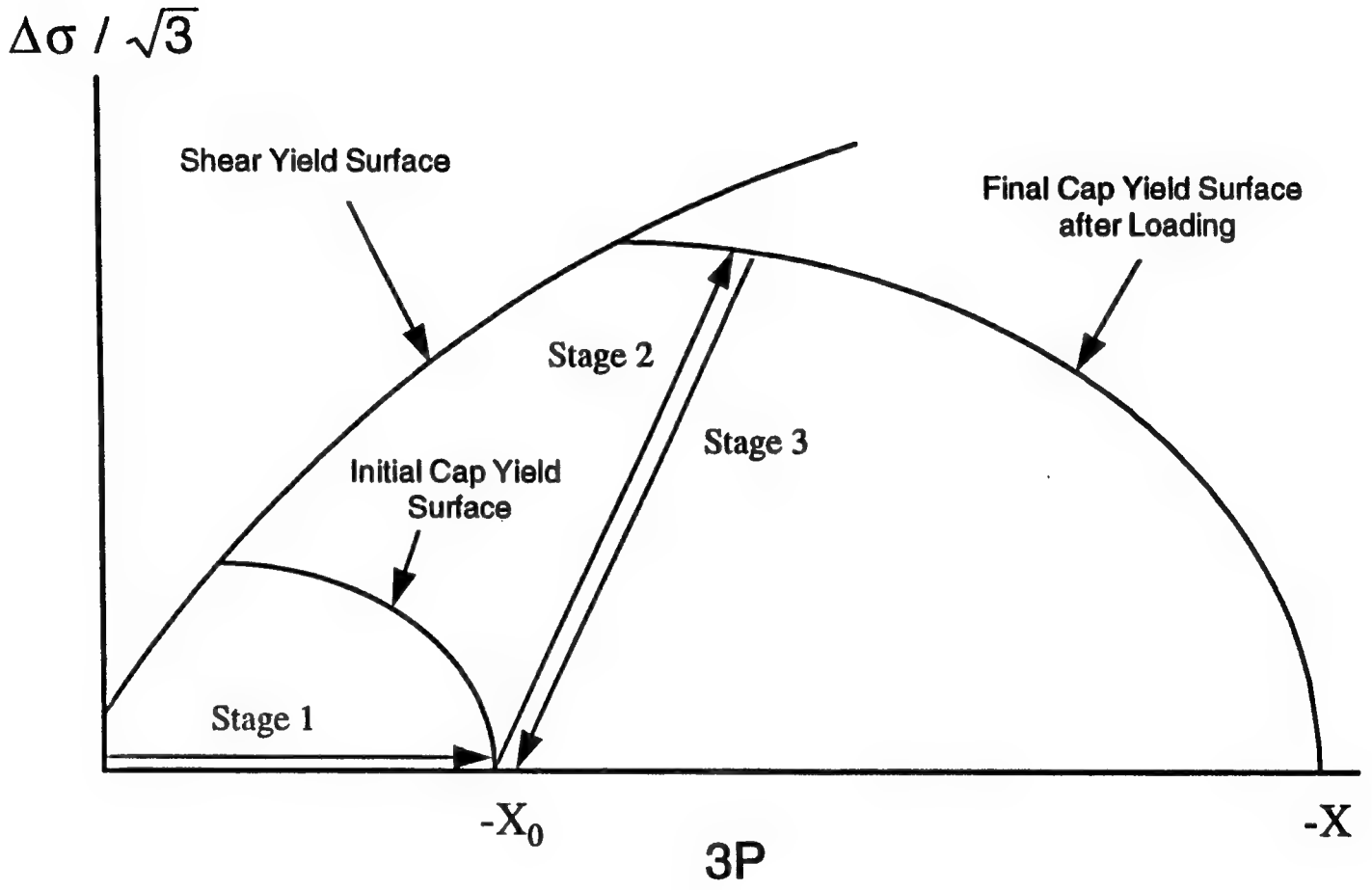

Figure 3-2. Three-stage load paths and their positions relative to yield surfaces.

3.4 TEST PROCEDURE.

An instrumented specimen is placed inside the pressure vessel of the test system. The pressure vessel is then filled with silicone oil and a small compressive hydrostatic preload (<1 MPa) is manually applied to the specimen by the system operator. Control of the test system is then given over to the computer. The control software requests operator input such as specimen dimensions, load path specifications, etc., and then begins to load the specimen. For hydrostatic/triaxial compression tests, the test system initially applies hydrostatic stress at a rate of -0.02 MPa/s (Stage 1, Figure 3-2). When the target hydrostatic stress is reached, the axial-load servo loop switches to axial strain control and axial loading continues at constant confining pressure at an axial strain rate of -1×10^{-5}/s (Stage 2, Figure 3-2). When approximately 85 percent of the physical range of the axial extensometer has been traversed, the axial-load servo loop switches back to load control and the stress difference and the hydrostatic stress are removed sequentially (Stage 3, Figure 3-2). For uniaxial strain tests, axial load is again applied in axial strain control; however, lateral straining is constrained by increasing confining pressure. The axial extensometer is used as feedback for the axial load servo loop, while the circumferential extensometer is used as feedback for the confining pressure servo loop. The imposed axial strain rate is -1×10^{-6}/s, which is one order of magnitude lower than used in the hydrostatic/triaxial compression tests. This lower strain rate is used to prevent high confining pressure rates that would result in adiabatic heating of the direct-contact extensometers. Uniaxial strain loading continues until the full range of the confining pressure transducer is traversed at which time the algebraic sign of the axial strain rate is reversed and the specimen is unloaded.

During both the hydrostatic/triaxial compression tests and the uniaxial strain tests, data are acquired based on the output levels of both the axial extensometer and the internal load cell. When the output of either of the transducers changes by more than 0.01 percent of full scale (based on physical range), data are logged. Logged data include time, axial load, confining pressure, axial deformation, and circumferential deformation. A typical datafile for a hydrostatic/triaxial compression test contains about 1,000 data points.

Data reduction is performed using a commercial spreadsheet software package. In this study, strains are true, or logarithmic strains, and stresses are true, or Cauchy stresses; i.e.,

the instantaneous dimensions of the specimen as determined from the deformation measurements are used to calculate stress.

In the model fitting procedure, the number of data points for each test is reduced from about 1,000 points to 30 points for each of the three loading stages (hydrostatic compression, triaxial compression loading, and triaxial compression unloading) for a total of 90 points per specimen. The number of points is reduced for reasons of practicality and to place equal weight on each stage of the load path. Data points are selected at equally spaced intervals within the original datafile using the algorithm, $I = (N - 1)/29$ where I is the interval between selected data points and N is the total number of data points acquired for a given stage of the load path. Therefore, if 1,000 points are contained within the original datafile, the interval between selected data points is 34. The first and last data point of each stage are always included in the reduced datafile.

3.5 EXPERIMENTAL RESULTS.

Figures 3-3 and 3-4 show the stress-strain data from all 20 tests. Axial stress is plotted against total axial, lateral, and volumetric strains. These figures illustrate the relatively small variability in the material. The inelastic strain in these tests is clearly the result of volume compaction as shown in the unloading portion of the stress-volumetric strain curves. Figure 3-5 shows peak values of $\Delta\sigma/\sqrt{3}$ plotted against $3P$ for the "walkdown" testing stages of the tests. The data indicate that the shear limit surface is concave toward the $3P$ axis. Figure 3-6, using data from one of the test specimens, illustrates the type of stress-strain behavior exhibited by each test specimen during the "walkdown" stages of the tests. From these stress-strain plots one can clearly see the relatively ductile nature of this limestone.

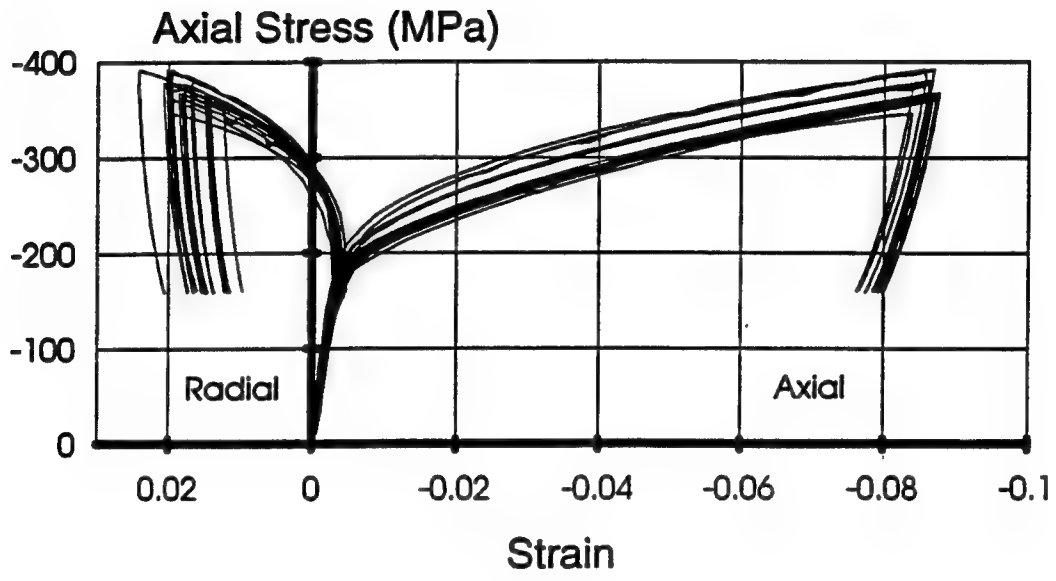

Figure 3-3. Axial stress versus axial strain and radial strain for all hydrostatic/triaxial compression tests.

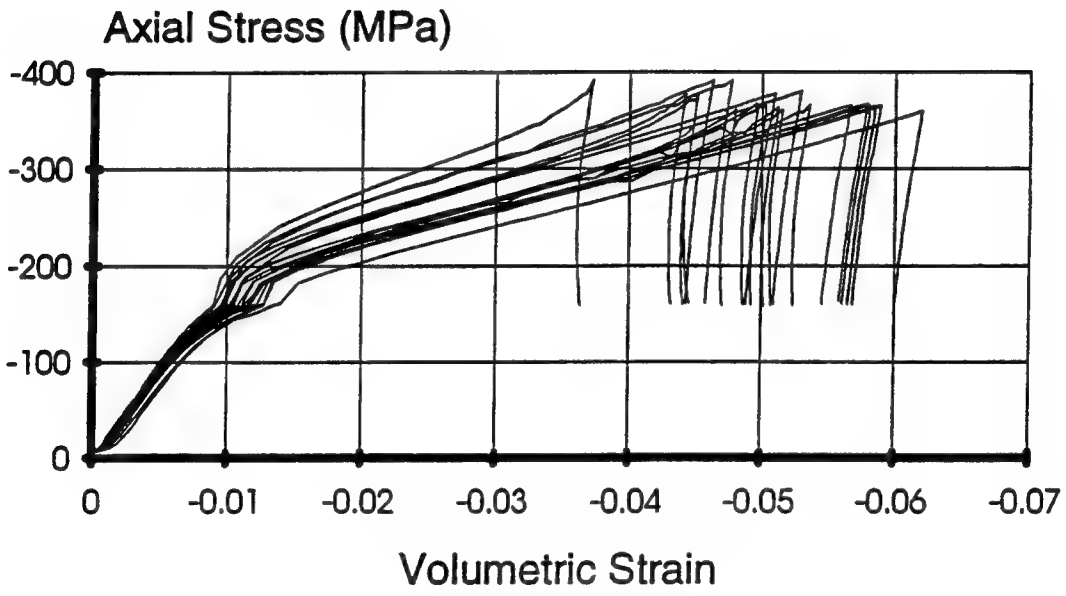

Figure 3-4. Axial stress versus volumetric strain for all hydrostatic/triaxial compression tests.

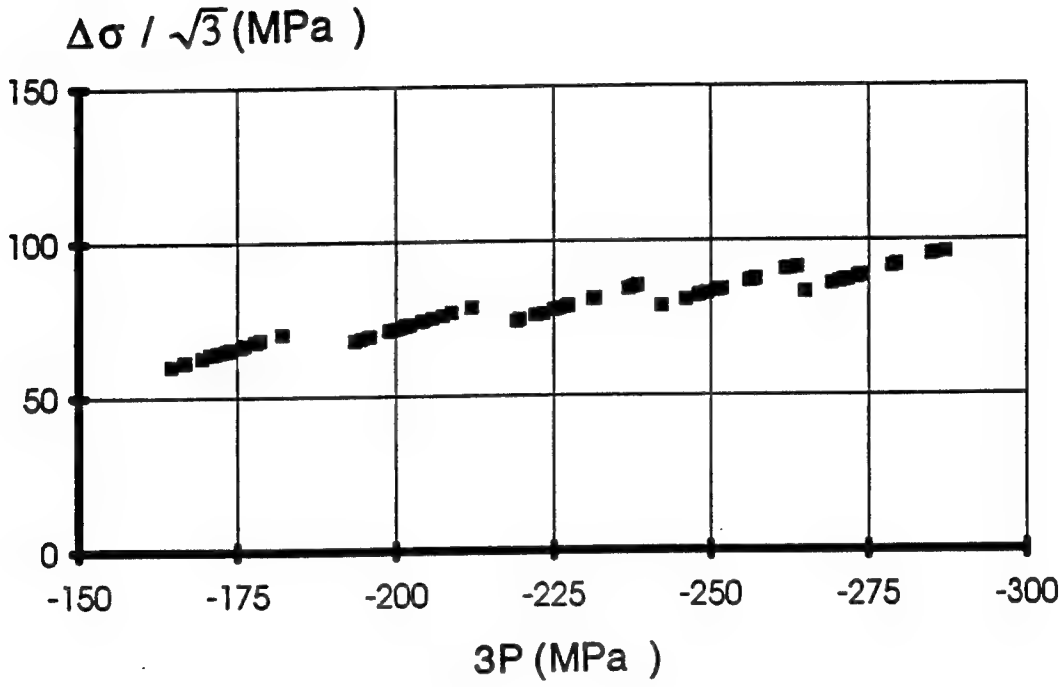

Figure 3-5. Peak values of $\Delta\sigma/\sqrt{3}$ plotted against $3P$ for the "walkdown" stages of the ultimate shear tests.

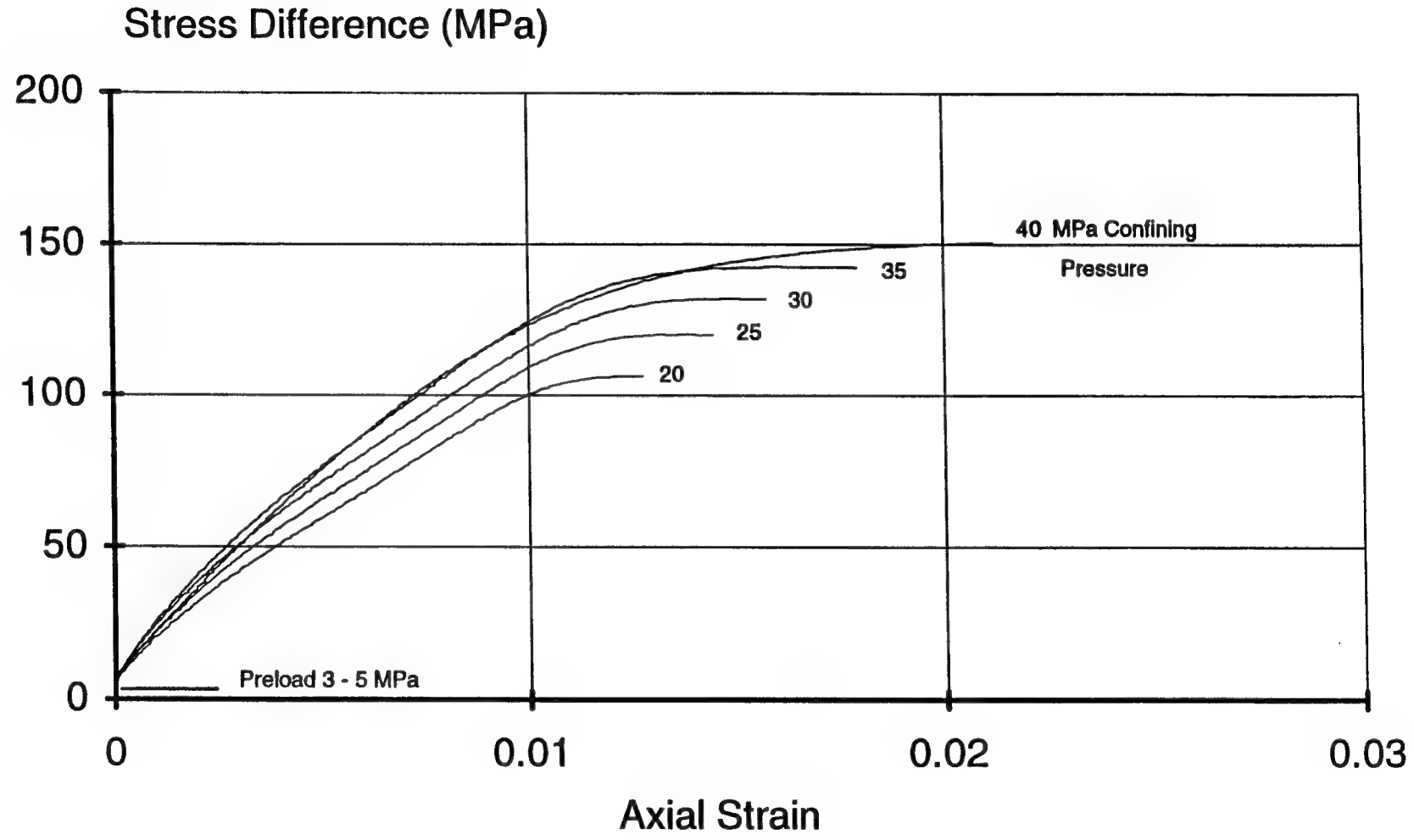

Figure 3-6. Stress-strain behavior during the "walkdown" stages of the ultimate shear tests.

SECTION 4

PARAMETER ESTIMATION/STATISTICAL PROPERTIES/DISTRIBUTIONS

4.1 MODEL FITTING PROCEDURE.

In the global nonlinear regression analysis, data from all stages of a single-specimen test are fitted simultaneously using response models appropriate for the load path followed in each testing stage. Different response models are required for each stage because different quantities are controlled during each stage. The objective function minimized in fitting the cap model is the weighted sum of squared residuals (*RSS*) given by

$$
\begin{aligned}
RSS = & \left\{ \sum_{i=1}^{30} (1/\|e_{kk}\|)^2 \, (\varepsilon^i_{kk_m} - \varepsilon^i_{kk_p})^2 \right\}_{STAGE\ 1} \\
& + \left\{ \sum_{i=1}^{30} (1/\|\sigma_{33}\|)^2 \, (\sigma^i_{33_m} - \sigma^i_{33_p})^2 + \sum_{i=1}^{30} (1/\|e_{11}\|)^2 \, (\varepsilon^i_{11_m} - \varepsilon^i_{11_p})^2 \right\}_{STAGE\ 2} \\
& + \left\{ \sum_{i=1}^{30} (1/\|e_{11}\|)^2 \, (\varepsilon^i_{11_m} - \varepsilon^i_{11_p})^2 + \sum_{i=1}^{30} (1/\|e_{33}\|)^2 \, (\varepsilon^i_{33_m} - \varepsilon^i_{33_p})^2 \right\}_{STAGE\ 3} \\
& + \left\{ 6 \cdot \sum_{i=1}^{5} (1/\|\Delta\sigma\|)^2 \, (\Delta\sigma^i{}_m - \Delta\sigma^i{}_p)^2 \right\}_{SHEAR\ STAGES}
\end{aligned}
\tag{4.1}
$$

in which the subscript m denotes "measured" and the subscript p denotes "predicted." Terms enclosed in double vertical lines are maximum measured values for the variable indicated and serve as weighting functions.

Total volumetric strain, ε_{kk}, is the dependent variable in Stage 1; axial stress, σ_{33}, and radial strain, ε_{11}, are the dependent variables in Stage 2; radial strain, ε_{11}, and axial strain, ε_{33}, are the dependent variables in Stage 3; and $\Delta\sigma$ is the dependent variable in the ultimate shear stages. A weighted least squares estimation rather than a standard least squares estimation is used because error variance is not homogeneous. Weighting also accounts for different units in the response model and thereby normalizes all test informa-

tion. In addition, since there are only five data points in each shear stage, the shear stages are multiplied by 6 so that each loading stage is weighted equally.

The Bio Medical Data Processing (BMDP) statistical software package, (BMDP Statistical Software, Inc., 1992), is used to solve for the response and to fit the model to laboratory data. A 5th-order Runge-Kutta integration method is used together with a pseudo-Gauss-Newton algorithm to perform nonlinear least squares fitting. The regression analysis gives estimates of each parameter, standard error for each parameter, and the correlation matrix of parameter estimates.

4.2 PARAMETER ESTIMATES.

The weighted least squares routine is applied to the objective function defined by Equation 4.1 for each of the 20 single specimen tests. Parameter estimates for each specimen are given in Table 4-1. The average coefficient of variation for the parameters is 30 percent. The highest correlation between parameters exists between A and C with a correlation coefficient near 1.0. The elastic parameters show the least correlation with other parameters. In general, a correlation coefficient near ± 1.0 between two different parameters suggests that the set of fitted parameters may be unstable and that a condition of multicollinearity may exist so that these parameter values may not be unique. Two causes of multicollinearity are the following: (1) the model may inherently include parameters that depend on one another, and (2) the database may not be sufficient to evaluate certain model parameters uniquely. To reduce multicollinearity, one could (*a*) modify the functional form of the model, or (*b*) expand the database of measurements. Nonetheless, because the correlation matrices are invertible, it is possible to transform the non-normal correlated parameters into statistically independent ones, (e.g., Liu and Der Kiureghian, 1986) for use in probabilistic analyses.

Figures 4-1 and 4-2 show, respectively, the model-fits to single-specimen stress-strain data with the lowest and highest *RSS* values, while Figures 4-3 and 4-4 show the corresponding model-fits to ultimate shear yield data from the same specimens. The best model-fit has an *RSS* value of 0.0403, while the worst model-fit has an *RSS* value of 0.0979. The median *RSS* value for the twenty specimens is 0.0637.

Table 4-1. Parameter estimates for each specimen.

Specimen Number	K(MPa)	G(MPa)	A(MPa)	B(1/MPa) E-03	C(MPa)	D(1/MPa) E-04	W	R	X_0(MPa)	RSS E-02
SL1214	14,562	8,613	209.89	1.810	198.80	8.262	0.071	5.88	-397.27	7.41
SL1231	18,472	10,878	217.04	1.523	190.07	5.986	0.059	6.18	-442.80	5.57
SL1232	16,710	9,593	220.29	1.471	195.76	9.786	0.058	5.90	-428.16	4.99
SL1241	16,432	8,941	209.04	1.648	190.52	15.76	0.054	6.00	-427.59	7.08
SL1242	15,679	8,893	212.86	1.696	201.69	12.87	0.059	5.98	-422.01	5.63
SL1243	16,824	9,765	186.28	1.868	166.45	9.756	0.071	5.57	-426.55	7.42
SL1244	15,802	10,168	205.08	1.683	186.00	19.80	0.052	5.98	-443.13	8.97
SL1245	15,181	10,143	193.58	1.869	175.83	14.58	0.074	5.03	-501.87	8.25
SL1246	14,401	8,558	186.29	2.018	171.83	2.803	0.250	5.19	-441.51	6.41
SL1251	16,805	9,882	210.23	1.801	198.90	12.95	0.059	5.91	-427.43	5.92
SL1253	17,902	9,854	196.15	1.777	181.33	15.31	0.048	6.35	-431.88	8.35
SL1255	16,758	9,259	209.61	1.787	198.49	3.909	0.189	5.63	-442.56	9.79
SL1261	17,378	10,802	216.36	1.712	201.72	6.524	0.074	5.95	-430.80	5.77
SL1265	16,846	9,399	213.01	1.723	196.30	7.084	0.102	5.03	-480.29	4.03
SL1266	17,357	9,461	197.26	2.107	189.54	3.008	0.191	5.49	-441.87	5.49
SL1275	13,671	8,670	154.38	2.998	152.92	7.790	0.115	5.34	-425.37	6.72
SL1276	16,071	9,094	191.12	2.120	183.41	3.372	0.226	5.10	-427.81	4.79
SL1278	13,527	8,414	185.44	2.244	181.96	4.342	0.167	5.27	-439.47	8.99
SL1713	17,385	9,674	203.57	1.947	190.08	5.410	0.100	5.06	-482.03	5.30
SL1715	16,511	10,559	171.06	2.648	163.84	3.003	0.144	5.66	-464.82	6.32

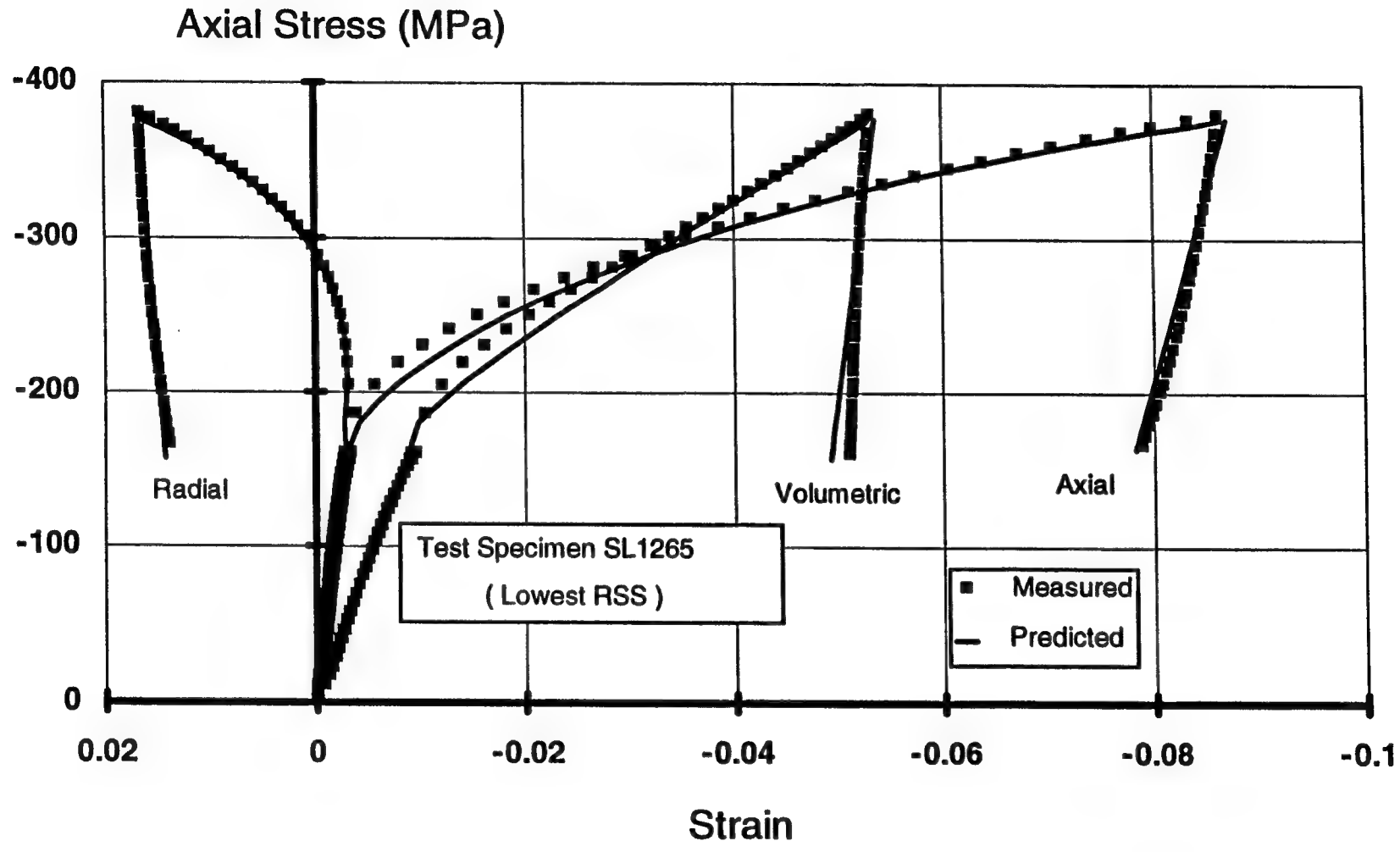

Figure 4-1. Lowest *RSS* model-fit to single-specimen stress-strain data.

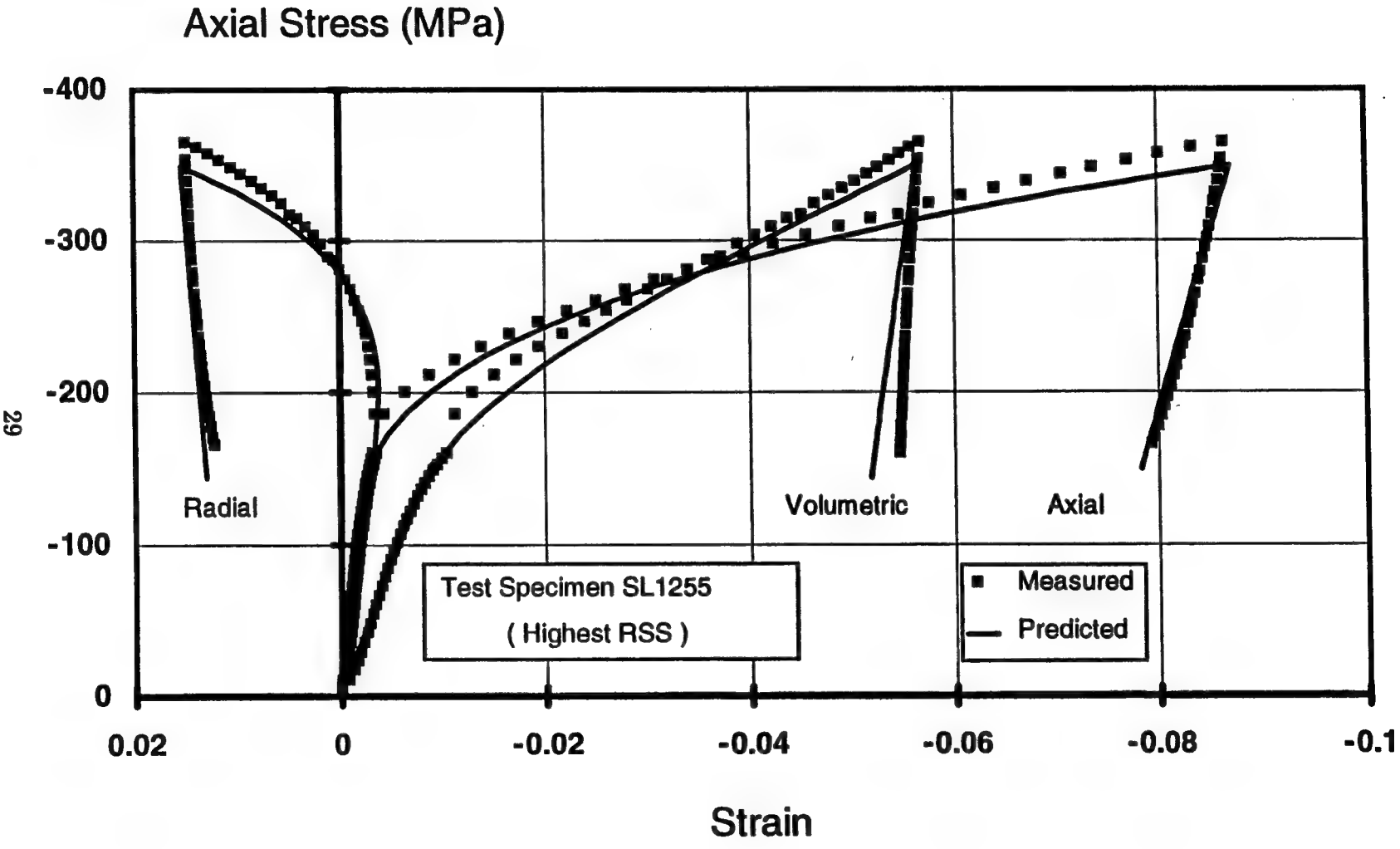

Figure 4-2. Highest *RSS* model-fit to single-specimen stress-strain data.

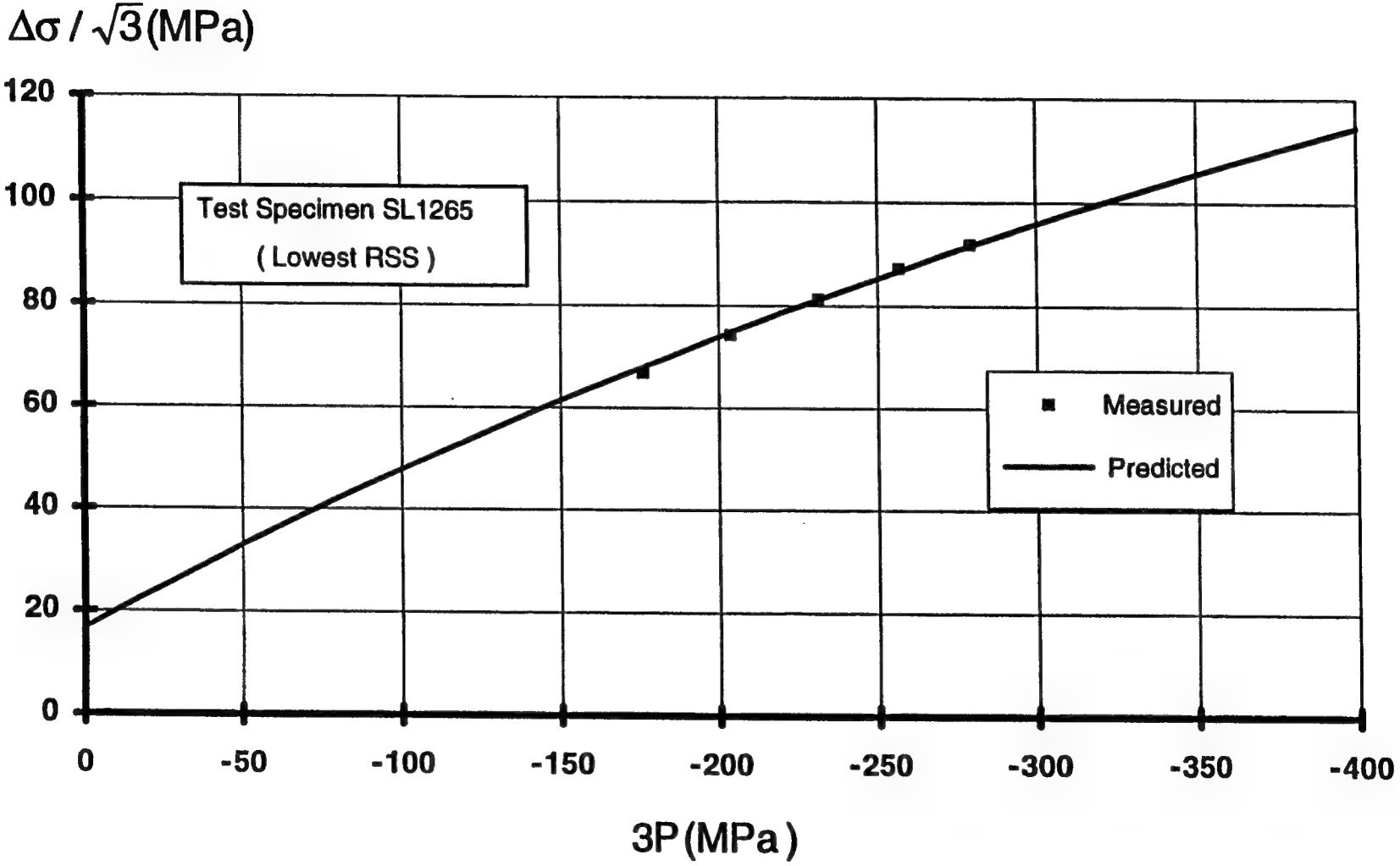

Figure 4-3. Lowest *RSS* model-fit to ultimate shear yield data from a single specimen.

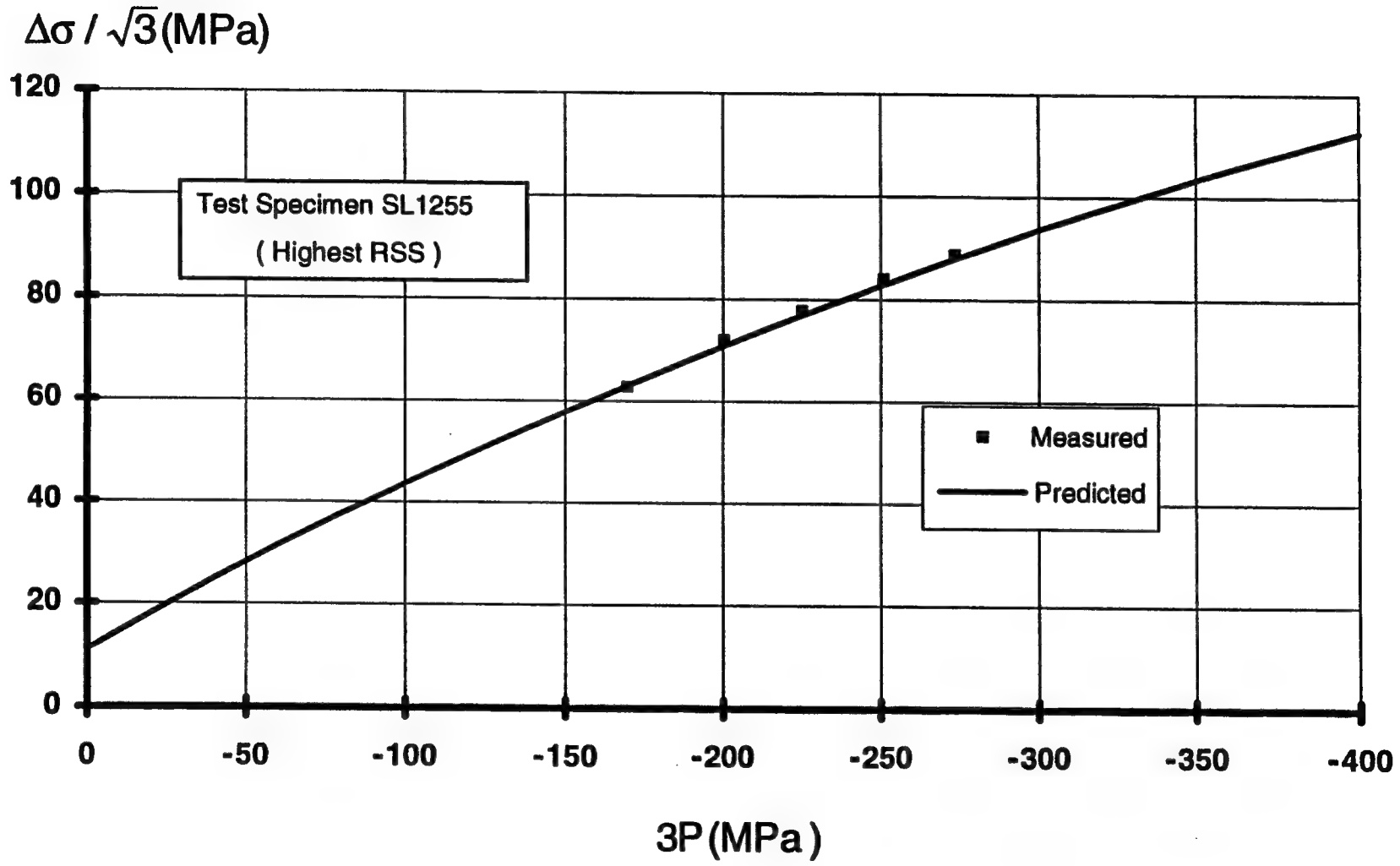

Figure 4-4. Highest *RSS* model-fit to ultimate shear yield data from a single specimen.

4.3 EVALUATION OF STATISTICAL PROPERTIES AND DISTRIBUTIONS.

To facilitate selection of probability density distribution functions, parameter estimates from the 20 tests are plotted as a frequency distribution in a graphic representation known as a histogram. The histogram breaks the total range into a series of intervals and indicates the numbers of occurrences into each interval by rectangles of different sizes. Representative of such a plot is the one for parameter *W* shown in Figure 4-5. In this case, indications are that functions skewed toward higher values of the random variable are appropriate. Distributions capable of capturing the skewed nature of the parameter are selected as candidates including lognormal, gamma, and Weibull (Type III - extreme value distribution). For comparison, we also include normal and uniform symmetric distributions. To discriminate among candidate functions, a statistic is needed to evaluate relative goodness-of-fit of each function against observed data. Two common statistics used for this purpose are the Chi-squared (χ^2) and Kolmogorov-Smirnov (*K-S*) tests for goodness-of-fit (Ang and Tang, 1975). The χ^2 statistic is a test on differences between hypothesized and observed frequencies within each interval of the histogram. The degrees of freedom in a χ^2 test depend on the number of intervals used to create the histogram. This means that the significance level for testing suitability of a proposed distribution function can vary depending on how the interval is chosen (Benjamin and Cornell, 1970). In addition, it is commonly recommended that at least five observations be recorded within each interval. The χ^2 test results become critically dependent on these factors for small sample sizes and conflicting results can occur even when the same data set is used to test a hypothesis and only the choice of histogram interval is varied.

An alternative to the χ^2 test is the *K-S* test that compares differences between hypothesized and observed cumulative distribution functions (*CDF's*). The degrees of freedom in the *K-S* test is unique and depends only on the number of data points used in the test. Because the number of parameter estimates is relatively small (20), the *K-S* test is chosen as the statistic to determine the relative goodness-of-fit of the candidate probability distribution functions. The largest difference between the experimental and predicted *CDF's* represents the *K-S* statistic, *D*.

The candidate probability density distribution functions are fitted to the histogram data depicted in Figure 4-5. Table 4-2 gives the *K-S* goodness-of-fit statistic for each of the

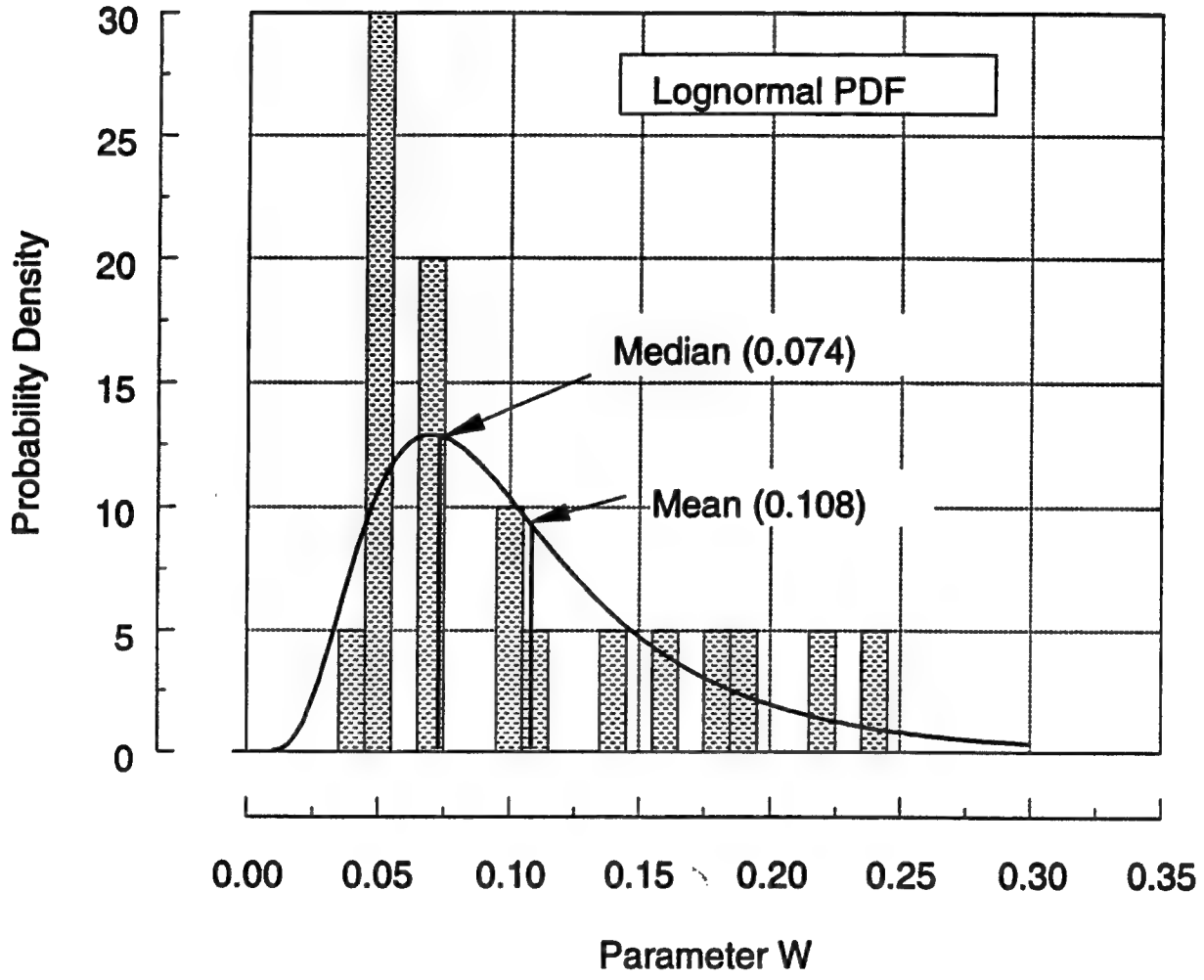

Figure 4-5. Histogram and probability function for parameter *W*.

Table 4-2. Candidate probability density functions and D statistic for parameter W.

CDF	D
Normal	0.255
Lognormal	0.218
Gamma	0.239
Weibull	0.233
Uniform	0.421

candidate probability density functions for parameter W. The table shows that the cumulative distribution function corresponding to the lognormal probability density function gives the lowest value of D. An illustration of how well the lognormal *CDF* fits the experimental *CDF* for W is shown in Figure 4-6. Figure 4-5 shows the lognormal probability density function superimposed on the histogram of parameter W. Distributions for the remaining parameters are determined in a similar fashion. A summary of these results is presented in Table 4-3 along with values for the mean, median, and standard deviation for each parameter.

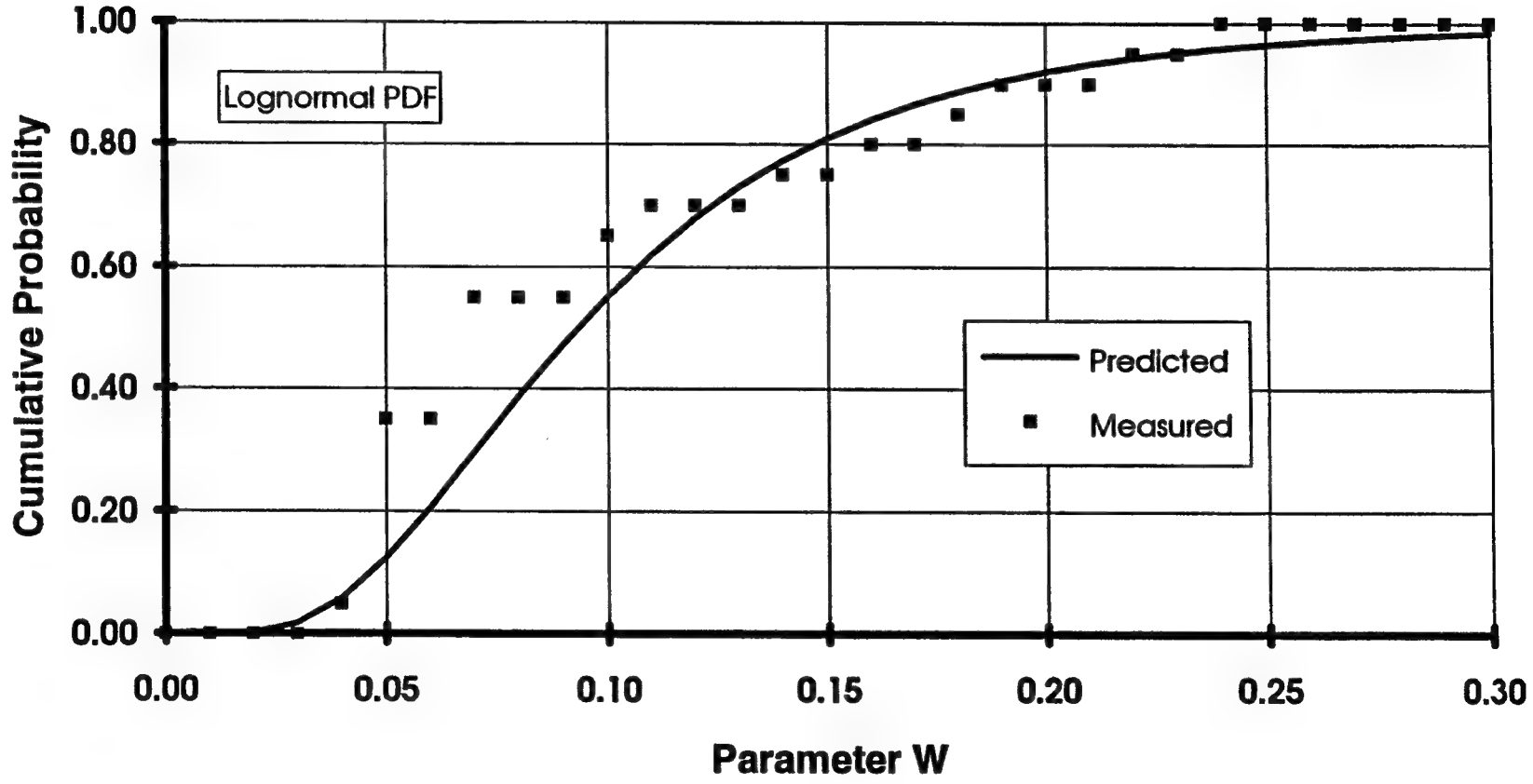

Figure 4-6. Comparison between predicted and experimental CDF for parameter *W*.

Table 4-3. Parameter distributions, statistics, and best-fit values.

Parameter	Probability Density Function	Mean Value	Standard Deviation	Median Value	Best-Fit Value
K (MPa)	Weibull	16,214	1,358	16,610	16,046
G (MPa)	Lognormal	9,531	740	9,527	10,093
A (MPa)	Weibull	199.43	16.80	204.32	269.52
B (1/MPa)	Lognormal	1.922E-03	3.680E-04	1.806E-03	1.211E-03
C (MPa)	Weibull	185.77	13.69	189.81	251.19
D (1/MPa)	Weibull	8.616E-04	5.055E-04	7.437E-04	6.410E-04
W	Lognormal	0.108	0.064	0.074	.109
R	Weibull	5.63	0.41	5.65	5.35
X_0 (MPa)	Lognormal	-441.26	24.20	-435.67	-458.60

SECTION 5

BEST FIT AND MODEL VALIDATION

5.1 OVERALL BEST-FIT PARAMETER ESTIMATES.

The best estimators of the true values of a set of parameters are those for which the fitted model gives the best fit, in a least squares sense, to the data considered simultaneously from all tests. That is, the objective function minimized in fitting the cap model includes twenty contributions, each one with a form identical to Equation 4.1. This set of parameters, shown in the last column of Table 4-3, is the best set to use in a deterministic analysis and are commonly called the "best-fit" parameters. From the overall fit, parameter X_0 has the lowest mean coefficient of variation at 5.48 percent, while parameter W has the highest value at 59.26 percent. Statistically, this means that parameters X_0 and W have the least and most uncertainty, respectively. Use is made of this set of parameters in the validation study.

The correlation matrix presented in Table 5-1 is determined from the overall best-fit calculations and is the one to use in probabilistic analyses that make use of the marginal probability distributions for the cap model parameters determined in Section 4.

5.2 VALIDATION AGAINST TESTS OUTSIDE THE FITTING DATABASE.

Because of the unconventional nature of the parameter estimation procedure, a validation study is used to assess the predictive capability of the fitted model. The overall best-fit parameter values are used to predict responses for tests and test types not included in the fitting database. These tests include triaxial compression tests at different constant confining pressures, uniaxial strain tests, and independent ultimate-shear tests conducted with multiple test specimens.

The first validation problem predicts hydrostatic/triaxial compression tests in which the specimen is loaded to -100 MPa in hydrostatic compression followed by axial straining to -8.5 percent in strain rate control. The confining pressure remains constant at -100 MPa. This test is identical to the first two stages of the tests discussed earlier except that the confining

Table 5-1. Matrix of correlation coefficients giving the degree of correlation among parameters.

	K	G	A	B	C	D	W	R	X_0
K	1.0000								
G	-0.0284	1.000							
A	0.0894	-0.0419	1.000			(Symmetric)			
B	-0.2610	0.0053	-0.9537	1.000					
C	0.0706	-0.0442	0.9997	-0.9511	1.000				
D	-0.0869	-0.2806	-0.6133	0.6406	-0.6166	1.000			
W	0.1161	0.2967	0.5996	-0.6270	0.6019	-0.9980	1.000		
R	-0.0679	-0.0785	-0.3943	0.2266	-0.3980	0.3028	-0.3001	1.000	
X_0	0.2618	-0.1251	0.7181	-0.8686	0.7157	-0.5423	0.5230	0.2270	1.000

pressure at the end of the first stage is -100 MPa rather than -150 MPa. Figure 5-1 shows measured versus predicted stress-strain behavior. Figures 5-2 and 5-3 show measured versus predicted results for similar tests in which the first stage ends at -50 MPa and 0 MPa respectively.

The next validation problem predicts the results of uniaxial strain tests. In this test the confining pressure is increased so that the radial strain is constrained to be zero while the axial strain increases. Figure 5-4 shows the results of ten uniaxial strain tests versus the predicted stress-strain behavior made with the best-fit parameters determined previously. Note that the prediction appears to give a best-fit to the uniaxial strain data even though this test type was not included in the fitting database.

The final validation exercise involves ultimate shear yield tests in which a different specimen is used for each of the different confining pressures used to define the yield envelope. The measured versus predicted results are shown in Figure 5-5. Each of the measured data points is taken from a different specimen. The predicted results make use of the best-fit parameters listed in Table 4-3 determined from replicated tests that included the "walk-down" load histories.

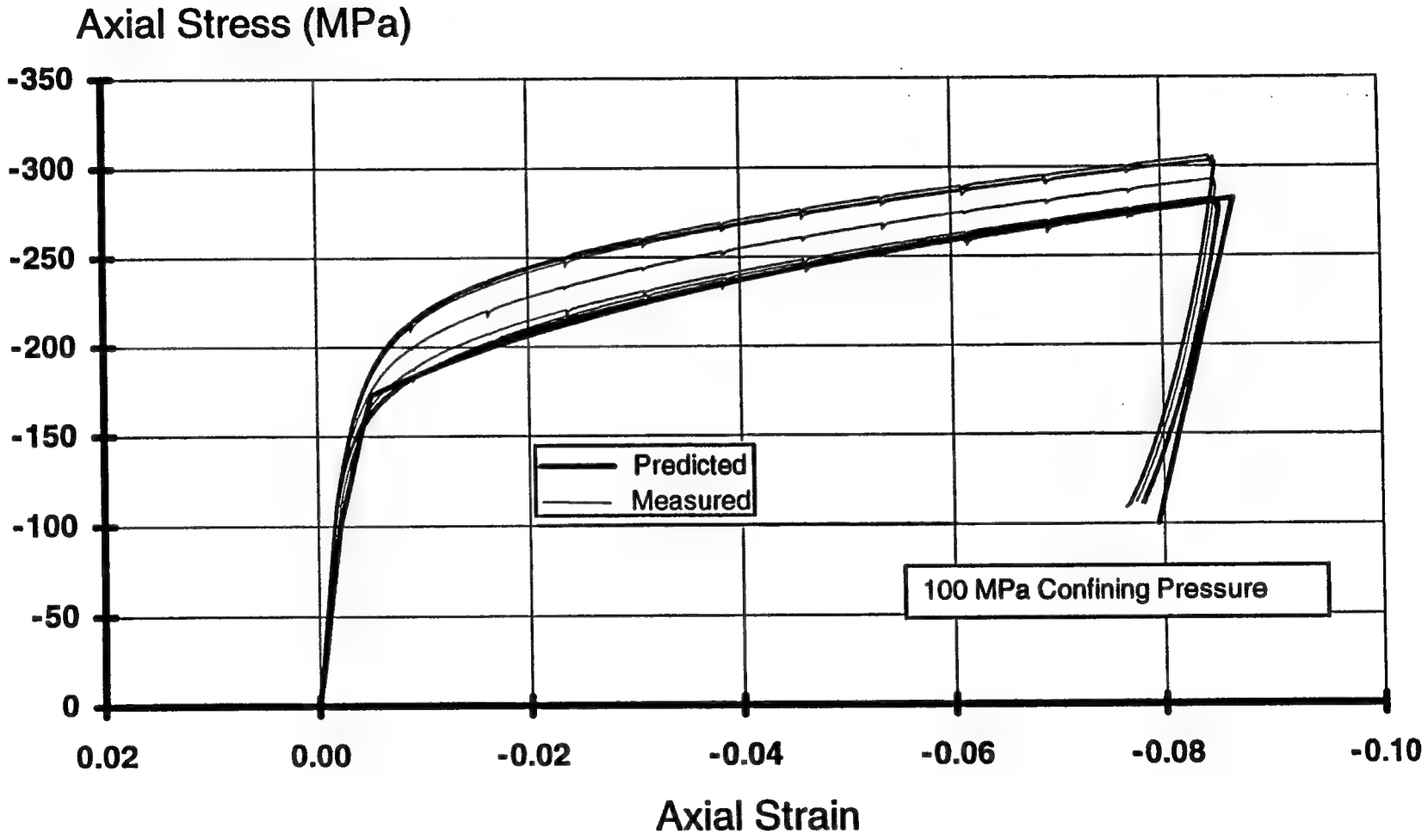

Figure 5-1. Predicted versus measured stress-strain behavior for the hydrostatic/triaxial compression validation tests conducted at a confining pressure of -100 MPa.

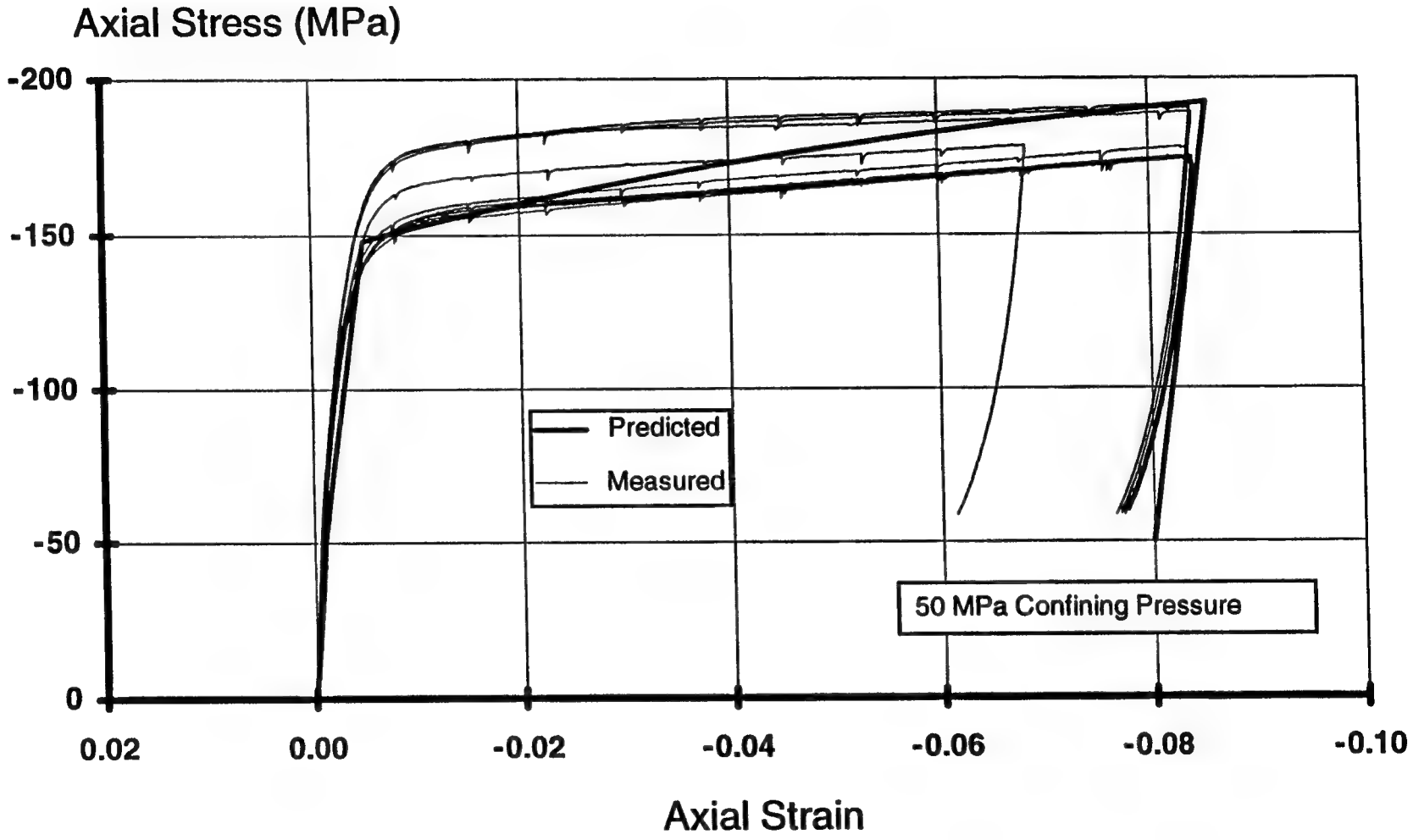

Figure 5-2. Predicted versus measured stress-strain behavior for the hydrostatic/triaxial compression validation tests conducted at a confining pressure of -50 MPa.

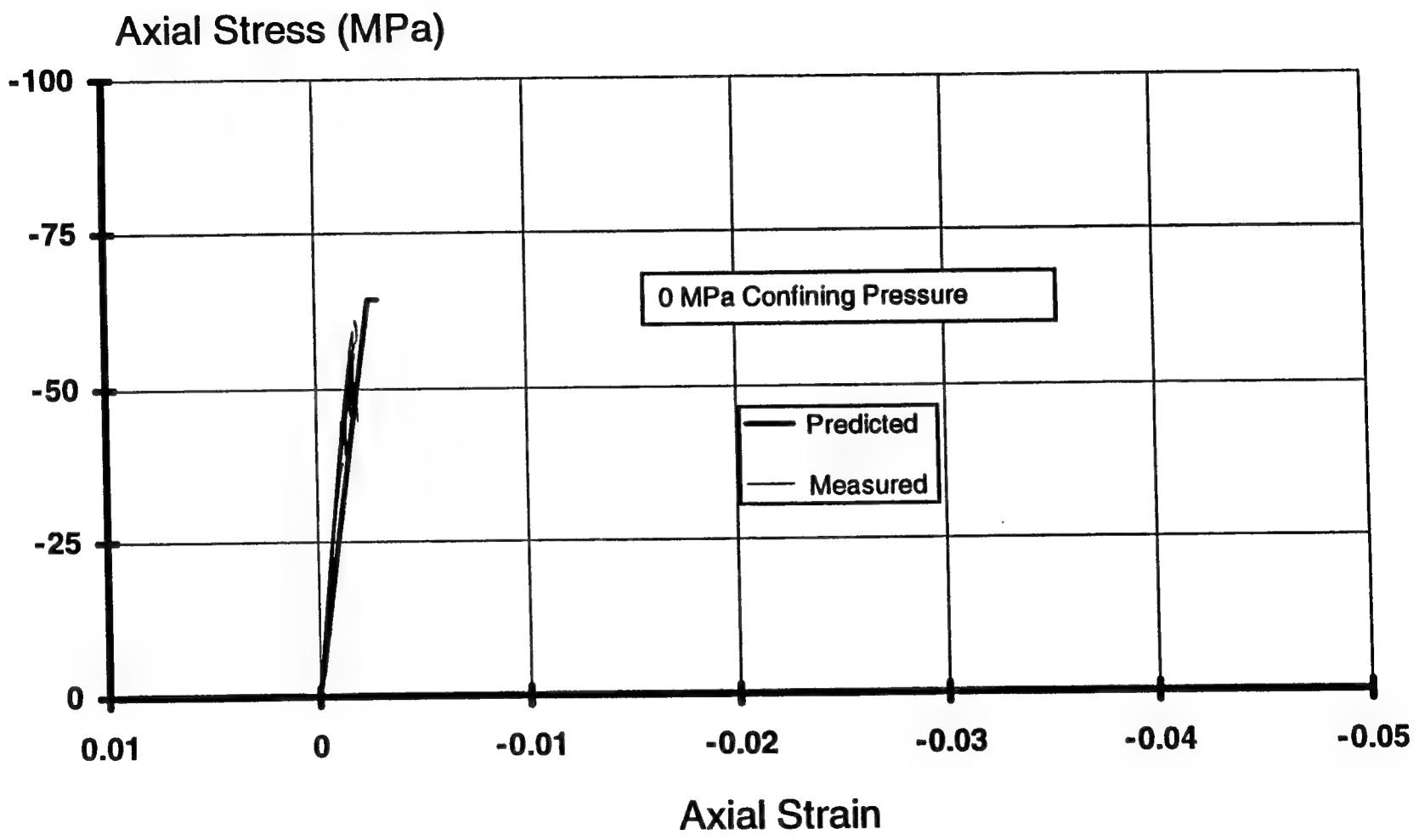

Figure 5-3. Predicted versus measured stress-strain behavior for the hydrostatic/triaxial compression validation tests conducted at zero confining pressure.

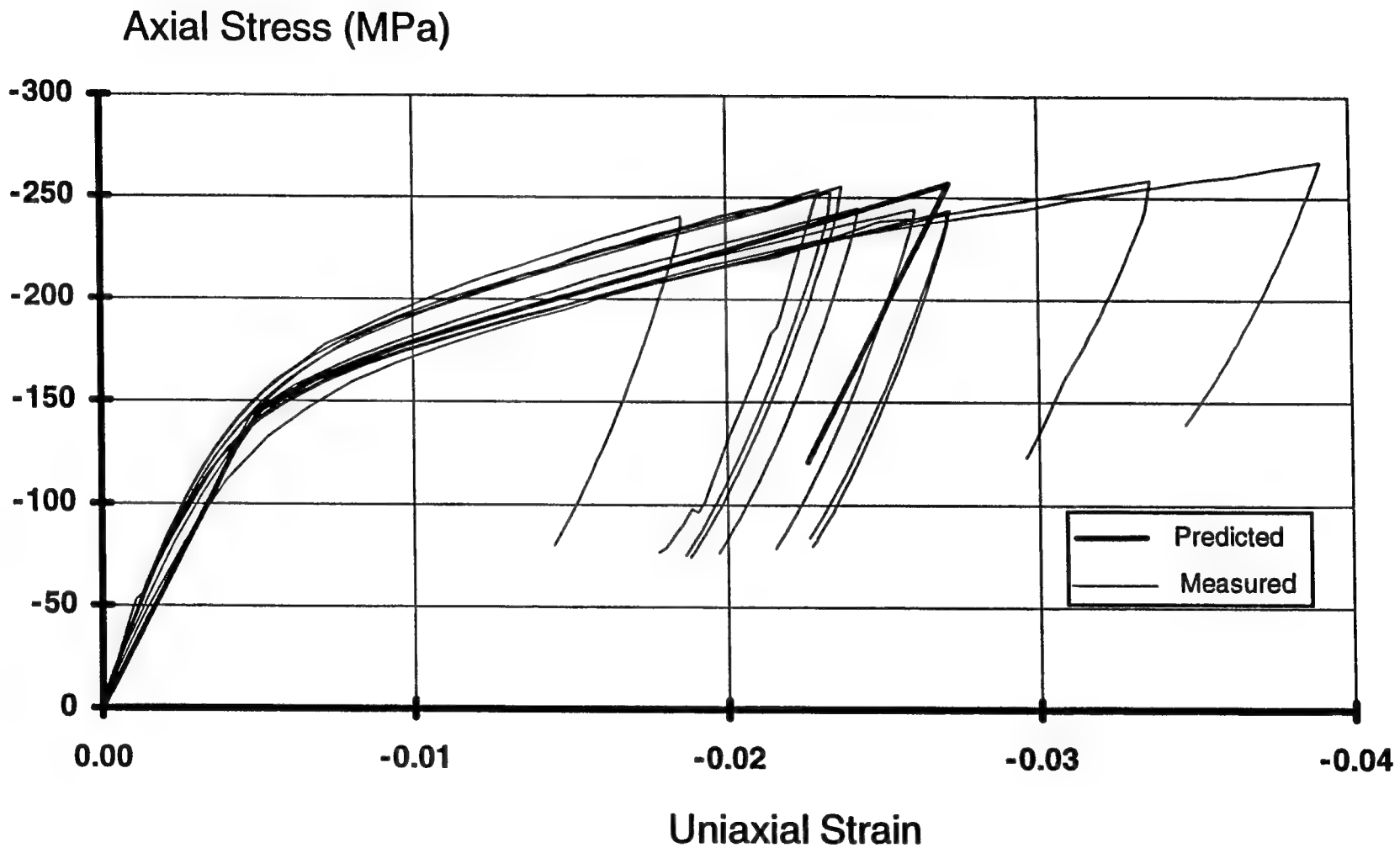

Figure 5-4. Predicted versus measured stress-strain behavior for the uniaxial strain validation tests.

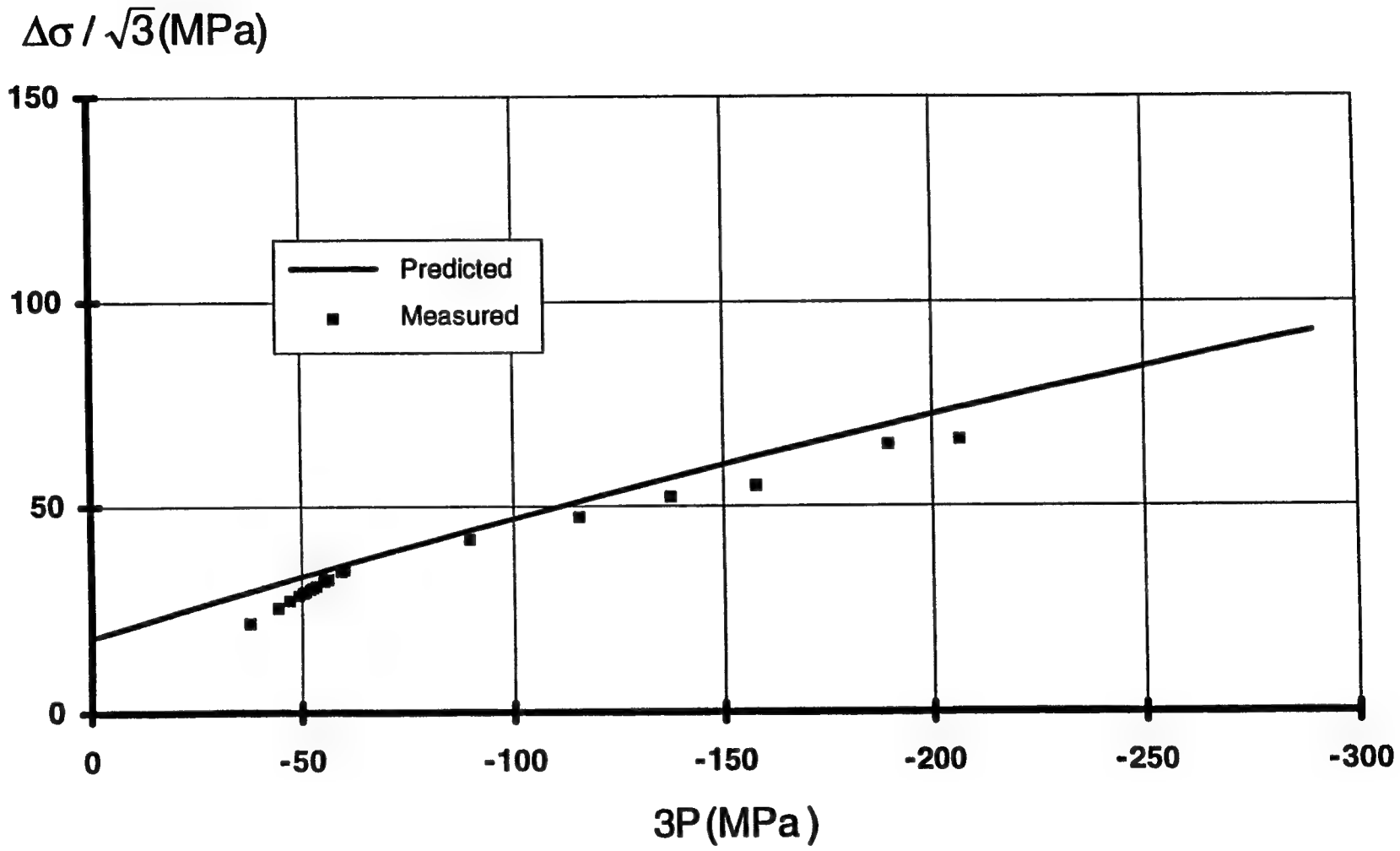

Figure 5-5. Predicted versus measured values of $\Delta\sigma/\sqrt{3}$ plotted against $3P$ for the independent ultimate shear tests.

The validation results clearly demonstrate that the parameter estimation procedure produces high-quality parameter values, and that the fitted model can not only reproduce measured data included in the fitting database, but also predict responses from tests conducted under loading histories different from those found in the fitting database.

SECTION 6

DISCUSSION

Exceptional care was taken throughout this investigation to quantify inherent variability in Salem limestone by minimizing estimation error, human error, and modeling error. Carefully controlled laboratory tests generate data for parameter evaluation. Response models are constructed corresponding to each test and best estimates of the model parameters are provided by the best fit to the data in a least squares sense. No *a priori* assumptions are required regarding the material behavior in the laboratory tests. All parameters are evaluated simultaneously to produce a consistent parameter set. By using a single specimen to determine a complete set of cap model parameters, statistical properties are determined by straightforward replication, thereby avoiding the complicating assumptions of simulation methods involving repeated use of data. Such methods may be unavoidable, however, as the level of model sophistication increases (e.g., accounting for the effects of unloading-reloading using a combination of isotropic and kinematic plastic hardening rules, or simulating the change in shape of the failure surface with the mean stress). In such cases, Monte Carlo computer simulation may be needed to simulate a series of experiments. This series could then be replicated as many times as necessary to obtain the relevant properties of the sampling distribution.

SECTION 7

CONCLUSIONS

Marginal probability distributions and a correlation matrix were presented for parameters of a cap plasticity material model. Point estimates of the parameters were determined by a testing scheme and parameter estimation procedure in which the parameters were determined from a single specimen. Statistical properties were determined from replicate testing, and probability distributions were determined from candidate distributions that best characterized parameter histograms.

SECTION 8

REFERENCES

Abduljauwad, Sahel N., Isa M. Al-Buraim, and Hamdan N. Al-Ghamedy, "Mixed Hardening, Three-Invariants Dependent Cap Model," *Journal of Engineering Mechanics*, Vol. 118, p. 620, 1992. (UNCLASSIFIED)

Ang, A. H.-S. and W.H. Tang, *Probability Concepts in Engineering Planning and Design, Vol. 1, Basic Principles,* John Wiley & Sons, 1975. (UNCLASSIFIED)

ANSI/ASME PTC 19.1-1985, *Part 1 Measurement Uncertainty: Instruments and Apparatus,* ASME, New York, NY, 1986. (UNCLASSIFIED)

ASTM, Standard Practice for Preparing Rock Core Specimens and Determining Dimensional and Shape Tolerances, *Annual Book of ASTM Standards,* Standard D4543-85, Vol. 04.04, Philadelphia, PA, 1988. (UNCLASSIFIED)

ASTM, Standard Test Method for Triaxial Compressive Strength of Undrained Rock Core Specimens Without Pore Pressure Measurements, *Annual Book of ASTM Standards,* Standard D2664-86, Vol. 04.04, Philadelphia, PA, 1989. (UNCLASSIFIED)

ASTM Institute for Standards Research, *Interlaboratory Testing Program for Rock Properties - Round I*, Philadelphia, PA, ISR PS #D18.12-Ro1, p. 15, 1992. (UNCLASSIFIED)

Baladi, G. and P. Hadala, *Isotropic Soil Cap Constitutive Model Equations and Fitting Parameter Value for use in Pre-Mine Throw IV Ground Shock Calculations*, Report to DNA, U.S. Army Engineer Waterway Experiment Station, Vicksburg, MS, 1974. (UNCLASSIFIED)

Baladi, George Y. and Behzad Rohani, "Elastic-Plastic Model for Saturated Sand," *Journal of Geotechnical Engineering*, Vol. 105, p. 465, 1979. (UNCLASSIFIED)

Baron, M.L., I. Nelson, and I. Sandler, "Influence of Constitutive Models of Ground Motion Predictions," *Journal of Engineering Mechanics,* Vol. 99, p. 1181, 1973. (UNCLASSIFIED)

Benjamin, J.R., and C.A. Cornell, *Probability, Statistics, and Decision for Civil Engineers*, McGraw-Hill, 1970. (UNCLASSIFIED)

BMDP Statistical Software, Inc., *BMDP/386 Dynamic User's Guide*, Los Angeles, CA, 1992. (UNCLASSIFIED)

Celle, C.C. and J.B. Cheatham, "Anisotropic Hardening of an Initially Isotropic Porous Limestone," *Rock Mechanics*, Vol 13, p. 221, 1981. (UNCLASSIFIED)

Cheatham, J.B. Jr., M.B. Allen, and C.C. Celle, "Kinematic Hardening of a Porous Limestone," *Rock Mechanics and Rock Engineering,* Vol. 17, p. 233, 1984. (UNCLASSIFIED)

Chu, H.S. and H. Brandt, "Constants for an elastic-Plastic Cap Model for Limestone," *International Journal for Numerical and Analytical Methods in Geomechanics*, Vol. 11, p. 193, 1987. (UNCLASSIFIED)

DiMaggio, F.L. and I.S. Sandler, "Material Model for Granular Soils," *Journal of Engineering Mechanics*, Vol. 97, p. 935, 1971. (UNCLASSIFIED)

Drucker, D.C., R.E. Gibson, and D.J. Henkel, "Soil Mechanics and Workhardening Theories of Plasticity," *Transactions of the A.S.C.E.*, Vol. 122, p. 338, 1957. (UNCLASSIFIED)

Fossum, A.F. and D.E. Munson, "Probabilistic Creep Analysis of an Underground Structure in Salt," (Submitted for Publication), 1994. (UNCLASSIFIED)

Fossum, A.F., P.E. Senseny, and B.H. Thacker, "Input Uncertainties and Calculated Borehole Closure," in: J-C. Roegiers (ed.), *Rock Mechanics as a Multidisciplinary Science*, A.A. Balkema, Rotterdam, p. 987, 1991. (UNCLASSIFIED)

Harren, S.V. and A.F. Fossum, "Probabilistic Analysis of an Impulsively Loaded Deep-Based Structure, *International Journal for Numerical and Analytical Methods in Geomechanics*, Vol. 15, p. 513, 1991. (UNCLASSIFIED)

Hofstetter, G., J.C. Simo, and R.L. Taylor, "A Modified Cap Model: Closest Point Solution Algorithms," *Computers & Structures*, Vol. 46, p. 203, 1993. (UNCLASSIFIED)

Huang, Tien-Kuen and Wai-Fah Chen, "Simple Procedure for Determining Cap-Plasticity-Model Parameters," *Journal of Geotechnical Engineering*, Vol. 116, p. 492, 1990. (UNCLASSIFIED)

Katona, M.G. and M.A. Mulert, "A Viscoplastic Cap Model for Soils and Rock," in: C.S. Desai and R.H. Gallagher, eds., *Mechanics of Engineering Materials*, John Wiley & Sons Ltd., p. 335, 1984. (UNCLASSIFIED)

Katona, M.G., "Evaluation of Viscoplastic Cap Model," *Journal of Geotechnical Engineering*, Vol. 110, p. 1106, 1984. (UNCLASSIFIED)

Liu, P.-L. and A. Der Kiureghian, "Multivariate Distribution Models With Prescribed Marginals and Covariances," *Probabilistic Engineering Mechanics*, Vol. 1, p. 105, 1986. (UNCLASSIFIED)

McCarron, W.O. and W.F. Chen, "A Capped Plasticity Model Applied to Boston Blue Clay," *Canadian Geotechnical Journal*, Vol. 24, p. 630, 1987. (UNCLASSIFIED)

Mellegard, K.D., T.W. Pfeifle, A.F. Fossum, and P.E. Senseny, "Pressure and Flexible Membrane Effects on Direct-Contact Extensometer Measurements in Axisymmetric Compression Tests," *Journal of Testing and Evaluation*, Vol. 21, p. 530, 1993. (UNCLASSIFIED)

Miller, T.W. and J.B. Cheatham Jr., "A New Yield Condition and Hardening Rule for Rocks," *International Journal of Rock Mechanics and Mining Sciences*, Vol. 9, p. 453, 1972. (UNCLASSIFIED)

Resende, Luis and John B. Martin, "Formulation of Drucker-Prager Cap Model," *Journal of Engineering Mechanics*, Vol. 111, p. 855, 1985. (UNCLASSIFIED)

Rubin, M.B., "Elastic-Viscoplastic Model for Large Deformation of Soils," *Journal of Engineering Mechanics*, Vol. 116, p. 1995, 1990. (UNCLASSIFIED)

Sandler, I.S., The Cap Model for Static and Dynamic Problems," *17th U.S. Symposium on Rock Mechanics,* Snowbird, Utah, p. 1A2-1, 1976. (UNCLASSIFIED)

Sandler, I.S., F.L. DiMaggio, and G.Y. Baladi, "Generalized Cap Model for Geological Materials," *Journal of the Geotechnical Engineering,* Vol. 102, p. 683, 1976. (UNCLASSIFIED)

Sandler, I.S. and D. Rubin, "An Algorithm and a Modular Subroutine for the Cap Model," *International Journal for Numerical and Analytical Methods in Geomechanics,* Vol. 3, p. 173, 1979. (UNCLASSIFIED)

Schwer, Leonard E. and Yvonne D. Murray, "A Single Surface Three Invariant Cap Model With Mixed Hardening" (Submitted for publication). (UNCLASSIFIED)

Senseny, P.E., "Deformation Measurements in Rock Mechanics Using Direct-Contact Extensometers," presented at the *4th Annual Hostile Environments and High Temperature Measurements Conference*, SEM, Windsor Locks, CT, 1987. (UNCLASSIFIED)

Simo, Juan C., Jiann-Wen Ju, Karl S. Pister, and Robert L. Taylor, "An Assessment of the Cap Model: Consistent Return Algorithms and Rate-Dependent Extensions," *Journal of Engineering Mechanics*, Vol. 114, p. 191, 1988. (UNCLASSIFIED)

Yamada, Shoji E. and Ahmed S. Abou-Sayed, "Cap Model Guided by Energy Concept," *Journal of Geotechnical Engineering Division*, Vol. 105, p. 183, 1979. (UNCLASSIFIED)

DISTRIBUTION LIST

DNA-TR-94-39

DEPARTMENT OF DEFENSE

ASSISTANT TO THE SECRETARY OF DEFENSE
ATTN: EXECUTIVE ASSISTANT

DEFENSE INTELLIGENCE AGENCY
ATTN: PGI-4
ATTN: PGI-4B J DOPERALSKI

DEFENSE NUCLEAR AGENCY
2 CY ATTN: IMTS
ATTN: OPNA
ATTN: SPSD
ATTN: SPSD D PYLE
ATTN: SPSD P SENSENY

DEFENSE TECHNICAL INFORMATION CENTER
2 CY ATTN: DTIC/OC

FIELD COMMAND DEFENSE NUCLEAR AGENCY
ATTN: FCTO
ATTN: FCTOS
ATTN: FCTT DR BALADI

DEPARTMENT OF THE ARMY

ADVANCED RESEARCH PROJECT AGENCY
ATTN: DEFENSE SCIENCES OFFICE

U S ARMY CORPS OF ENGINEERS
ATTN: CERD-L

U S ARMY ENGINEER DIST OMAHA
ATTN: MROED-S H GAUBE

U S ARMY ENGR WATERWAYS EXPER STATION
ATTN: C D NORMAN
ATTN: CEWES J K INGRAM
ATTN: CEWES-SD
ATTN: CEWES-SE L K DAVIS
ATTN: CEWES-SS-R DR BALSARA
ATTN: DR D BANKS CEWES-GS
ATTN: G ALBRITTON
ATTN: J WARRINER WESGR-M
ATTN: RESEARCH LIBRARY
ATTN: W MILLER

DEPARTMENT OF THE AIR FORCE

AIR FORCE CTR FOR STUDIES & ANALYSIS
ATTN: AFSAA/SAI

AIR UNIVERSITY LIBRARY
ATTN: AUL-LSE

DEPARTMENT OF ENERGY

LOS ALAMOS NATIONAL LABORATORY
ATTN: REPORT LIBRARY

SANDIA NATIONAL LABORATORIES
ATTN: DIV 9311 L R HILL
ATTN: TECH LIB 3141
ATTN: 9312 C W SMITH

OTHER GOVERNMENT

CENTRAL INTELLIGENCE AGENCY
ATTN: OSWR/NED 5S09 NHB

DEPARTMENT OF THE INTERIOR
ATTN: P SANDS

DEPARTMENT OF DEFENSE CONTRACTORS

AEROSPACE CORP
ATTN: LIBRARY ACQUISITION

ANALYTIC SERVICES, INC (ANSER)
ATTN: K BAKER

APPLIED RESEARCH ASSOCIATES, INC
ATTN: C J HIGGINS

APPLIED RESEARCH ASSOCIATES, INC
ATTN: S BLOUIN

APPLIED RESEARCH ASSOCIATES, INC
ATTN: R FRANK

BDM ENGINEERING SERVICES CO
ATTN: D BURGESS

BOEING TECHNICAL & MANAGEMENT SVCS, INC
ATTN: W M LEAVENS
ATTN: A W SPENCER
ATTN: R BRYAN CAIRNS

IIT RESEARCH INSTITUTE
ATTN: DOCUMENTS LIBRARY
ATTN: M JOHNSON

INSTITUTE FOR DEFENSE ANALYSES
ATTN: CLASSIFIED LIBRARY

JAYCOR
ATTN: CYRUS P KNOWLES

KAMAN SCIENCES CORP
ATTN: RICHARD KEEFFE

KAMAN SCIENCES CORP
ATTN: DASIAC

KAMAN SCIENCES CORPORATION
ATTN: DASIAC

LACHEL AND ASSOCIATES, INC
ATTN: C LINAMEN
ATTN: J BECK

LOGICON R & D ASSOCIATES
ATTN: LIBRARY

LOGICON R & D ASSOCIATES
ATTN: J WALTON

LOGICON R & D ASSOCIATES
ATTN: D PIEPENBURG

MAXWELL LABORATORIES INC
ATTN: K D PYATT JR

NTS ENGINEERING
ATTN: S SHORT

PACIFIC-SIERRA RESEARCH CORP
ATTN: H BRODE

PACIFIC-SIERRA RESEARCH CORP
ATTN: D GORMLEY

RE/SPEC INC
2 CY ATTN: A F FOSSUM
2 CY ATTN: K D MELLEGARD
2 CY ATTN: T W PFEIFLE

SCIENCE APPLICATIONS INTL CORP
ATTN: DR M MCKAY
ATTN: H PRATT
ATTN: TECHNICAL REPORT SYSTEM

SCIENCE APPLICATIONS INTL CORP
ATTN: W LAYSON

SOUTHWEST RESEARCH INSTITUTE
ATTN: A FOSSUM
ATTN: B THACKER

SRI INTERNATIONAL
ATTN: J GRAN

TITAN CORPORATION
ATTN: J THOMSEN

TITAN CORPORATION (THE)
ATTN: LIBRARY
ATTN: S SCHUSTER
ATTN: Y M ITO

TRW SPACE & DEFENSE SECTOR
ATTN: W WAMPLER

UTD, INC
ATTN: E FOSTER

WEIDLINGER ASSOC, INC
ATTN: H LEVINE

WEIDLINGER ASSOCIATES, INC
ATTN: I SANDLER
ATTN: M BARON